Lawrence Berkeley National Laboratory
Recent Work

Title
DIFFUSION OF XENON IN URANIUM MONOCARBIDE

Permalink
https://escholarship.org/uc/item/8m27k56z

Author
Shaked, Hagai.

Publication Date
1962-11-07

eScholarship.org Powered by the California Digital Library
University of California

UCRL-10462

University of California

Ernest O. Lawrence
Radiation Laboratory

TWO-WEEK LOAN COPY

This is a Library Circulating Copy which may be borrowed for two weeks. For a personal retention copy, call Tech. Info. Division, Ext. 5545

DIFFUSION OF XENON IN URANIUM MONOCARBIDE CRYSTALS

Berkeley, California

DISCLAIMER

This document was prepared as an account of work sponsored by the United States Government. While this document is believed to contain correct information, neither the United States Government nor any agency thereof, nor the Regents of the University of California, nor any of their employees, makes any warranty, express or implied, or assumes any legal responsibility for the accuracy, completeness, or usefulness of any information, apparatus, product, or process disclosed, or represents that its use would not infringe privately owned rights. Reference herein to any specific commercial product, process, or service by its trade name, trademark, manufacturer, or otherwise, does not necessarily constitute or imply its endorsement, recommendation, or favoring by the United States Government or any agency thereof, or the Regents of the University of California. The views and opinions of authors expressed herein do not necessarily state or reflect those of the United States Government or any agency thereof or the Regents of the University of California.

Research and Development

UCRL-10462
UC-4 Chemistry
TID 4500 (18th Ed.)

UNIVERSITY OF CALIFORNIA

Lawrence Radiation Laboratory
Berkeley, California

Contract No. W-7405-eng-48

DIFFUSION OF XENON IN URANIUM MONOCARBIDE

Hagai Shaked

(Ph. D. Thesis)

November 7, 1962

Printed in USA. Price $2.25. Available from the
Office of Technical Services
U. S. Department of Commerce
Washington 25, D.C.

DIFFUSION OF XENON IN URANIUM MONOCARBIDE

Contents

DIFFUSION OF XENON IN URANIUM MONOCARBIDE

Hagai Shaked

Inorganic Materials Research Division
of Lawrence Radiation Laboratory
and Department of Nuclear Engineering
University of California
Berkeley, California

November 7, 1962

ABSTRACT

The lattice diffusion coefficient of Xe^{133} in cast uranium monocarbide was measured in postirradiation anneal experiments in the temperature range 1000°C to 2000°C. This was the first time that diffusion coefficient of Xe^{133} in UC was measured above 1400°C, and it was found that the diffusion coefficient of specimens consisting of large grains (700 to 1000 microns) was best approximated by

$$D = (1.17 \pm 0.16)10^{-6} \exp\left[-\frac{54900 \pm 1200}{RT}\right]$$

in the range 1000°C to 2000°C. (The units of D are cm^2/sec, and RT is in units of cal/mole.) Specimens with small grains (20 to 150 microns) exhibited the same diffusion coefficient above 1500°C. Below 1500°C results with small-grained specimens varied widely, indicating dependence on grain size and, hence, existence of appreciable grain-boundary diffusion.

The specimens, which were 5×5-mm cylinders, were irradiated in evacuated pyrex capsules in the Livermore pool-type reactor, at levels ranging between 6×10^{14} and 3×10^{15} n/cm^2. After irradiation each specimen, contained in a tungsten cup, was annealed isothermally in an induction chamber for about 12 hours. Xe^{133} released from the annealed specimen was adsorbed on charcoal at liquid nitrogen temperature. The charcoal was continuously monitored with a scintilation detector during the anneal. Total Xe^{133} content of the specimen was determined by melting the specimen and collecting the xenon on the same charcoal trap.

In calculating D the "conventional" analysis, which has been applied in previous experiments and in which a uniform concentration of Xe^{133} at the start of the anneal is assumed, was replaced by a new analysis. In the new analysis account was taken of the nonuniformity in the concentration of Xe^{133} at the start of the anneal due to the recoil release during irradiation prior to the anneal. Diffusion coefficients obtained in this experiment are lower by one order of magnitude than those obtained by Lindner and Matzke for UC particles, and higher by two-and-a-half to three orders of magnitude than those obtained by Auskern and Osawa for UC powders. Values of D obtained here are of the same order of magnitude as obtained for the diffusion of Xe^{133} in urania.

I. INTRODUCTION

A. Fission Gas Release in Nuclear Fuels

The combined fission yield of stable and long-life isotopes of the noble gases xenon and krypton is 25 to 30%. At a typical irradiation level of 10,000 MWD/ton of UO_2 every 1 cc of fuel produces 3 cc of these gases at normal temperature and pressure. If all this gas were released to the fuel-cladding gap, a severe increase in pressure could result.[E1] It is for this reason that the ability to retain fission gas must be included in the criteria for a good nuclear fuel.

Several mechanisms are responsible for this release.

a. Diffusion. Whether by lattice or grain-boundary diffusion, the rate of release is determined by the diffusion coefficient D, where

$$D = D_0 \exp(-E/RT). \qquad (I-1)$$

Hence, release is highly dependent on temperature. Derivation of Eq. (I-1) and discussion of the various types of diffusion can be found in various places in the literature.[L1]

b. Pores and Cracks. Owing to temperature transients, closed pores and cracks may open up, or open pores and cracks may close, hence affecting the release.

c. Closed Pores. It has been found[L2] that closed pores migrate up a temperature gradient. Such a pore containing fission gas causes a burst of fission gas upon reaching an inner surface of the fuel body.

d. Knock out. A fission product at rest within the fuel may be knocked out by an energetic fission product.[L2]

e. Knock in. A fission product that already has been released to a pore or to the fuel-cladding gap may be knocked back into the fuel by an energetic fission product.[L2]

f. Fission Recoil. A fission product born close enough to the fuel surface may escape by fission recoil. This mechanism is discussed in Appendix A.

In this investigation we are concerned only with diffusion. Because the fission recoil affects the diffusion results, a solution to the fission-recoil problem is presented in Appendix A.

B. Experimental and Theoretical Work to Date

Fission-gas release has been measured in many experiments on UO_2 [B1] and other uranium-bearing specimens. These experiments can be classified into three types:

a. Postirradiation anneal, in which a previously irradiated specimen is vacuum-annealed isothermally; the amount of gases released is measured as a function of time.

b. Irradiation of a fuel specimen in an operating reactor; released gas is continuously collected and measured while the specimen is being irradiated.

c. Irradiation of a fuel specimen inside a sealed capsule; the amount of gas within the capsule is collected and measured after the irradiation.

We are concerned here only with the postirradiation-anneal type of experiment.

The theoretical analysis for this type of experiment, as well as results of numerous experiments on UO_2 specimens, is described in the literature. [B1]

We mention here the only two published postirradiation-anneal experiments on uranium monocarbide. Lindner and Matzke used small particles of UC obtained by crushing arc-cast UC, and covered the temperature range 800 to 1300°C. [L4] Auskern and Osawa used very fine powder (0.26 to 0.28 m^2/g) and covered the temperature range 1000 to 1400°C. [A2]

In analyzing the results of postirradiation anneal with powder or sintered specimens, a "spherical model" [B5] has been used. It is assumed in this model that the specimen consists of many spheres in which the concentration of fission gas at the end of irradiation is uniform. With the notation

$$\frac{\partial C}{\partial x} = C_x, \qquad \frac{\partial^2 C}{\partial x^2} = C_{xx}, \quad \text{etc.}$$

the Xe^{133} concentration C inside a sphere of radius a at time t after anneal started is given by

$$C_t = D\left[C_{rr} + \frac{2}{r} C_r\right], \quad \text{for } r < a, \ 0 < t, \tag{I-2a}$$

$$C(r, 0) = C_0, \quad \text{for } r < a, \tag{I-2b}$$

$$C(a, t) = 0, \quad \text{for } 0 \leq t. \tag{I-2c}$$

It is assumed, then, that the collection of spheres can be represented by a single "average" sphere of radius a. We define a fractional release f as the ratio of the total amount of gas released in time t to the total amount of that species present in the specimen at t = 0. The fractional release, f, is then calculated from the solution of Eqs. (I-2):

$$f \approx \frac{6}{\pi^{1/2}} \tau^{1/2}, \quad \tau = Dt/a^2, \quad \text{for } \tau < 0.01, \tag{I-3}$$

where a is the radius of the average sphere and is determined from the total (measured) surface area of the powder. This model has seemed to apply very well in many individual experiments. However, comparison between the different experiments shows a very wide spread in the results.[B1] There are three basic reasons for this spread:

a. There are differences in the methods of preparation and the histories of the specimens used in different experiments. This is a very important factor, since diffusion processes are in general extremely sensitive to impurities and to imperfections in crystal structure.

b. A gas-adsorption method is used to measure the surface area of the powder. It is possible that the surface area available for adsorption is different and not in a constant ratio to the surface available for diffusion.[L4]

c. The results are extremely sensitive to the distribution of grain size, in the case of large fractional release (as shown in Appendix F).

C. Objective and Approach in this Research

The objective of this research is to obtain the lattice diffusion coefficient for Xe^{133} in UC in the temperature range 1000° to 2000°C.

The diffusion coefficient is calculated from the measured fractional release in a postirradiation anneal. Specimens used are cast uranium carbide right cylinders, 0.5×0.5 cm. Grain size in some specimens is varied intentionally by high-temperature vacuum anneal prior to irradiation in order to investigate and isolate the effect of release via grain-boundary diffusion (see Section IV. D).

In the analysis it is assumed that release is from external surface area only (i. e., no pores or cracks). The fractional release is calculated by taking into account the nonuniform Xe^{133} concentration at the end of irradiation (see Section III. B). This nonuniformity is due to the escape of some Xe^{133} by fission recoil during irradiation (Appendix A).

The nonrecoil fractional release is

$$f_{nr} = (6/\pi^{1/2})\,\tau^{1/2} \qquad \text{for } \tau < 0.01 \qquad \text{(I-4)}$$

The fractional release with recoil as used in this analysis is

$$f = (3/\pi^{1/2})[1 + \Phi(\tau)]\,\tau^{1/2} \qquad \text{for } \tau < 0.01 \qquad \text{(I-5)}$$

or

$$\frac{f}{f_{nr}} = \frac{1 + \Phi}{2} \qquad \text{for } \tau < 0.01\,. \qquad \text{(I-6)}$$

An analytical expression for the recoil correction factor Φ is derived in Appendix B. The value of Φ is zero at the start of the anneal and asymptotically approaches unity as anneal time increases.

II. EXPERIMENTAL PROCEDURE

A. Introduction

A specimen of uranium monocarbide is given a short irradiation at low temperature. Then, it is vacuum annealed (in the apparatus shown in Fig. 5) at some fixed temperature between 1000°C and 2000°C. The anneal time is about 12 hours, and during this time fission gases are released from the specimen; some of these gases are adsorbed on a charcoal trap at liquid nitrogen temperature. Xe^{133} is one isotope among those collected on the charcoal trap. (The silver trap was introduced to stop isotopes of iodine, in particular the high-fission-yield I^{131}.) The Xe^{133} has a very high fission yield of about 6.5%; it is a gamma emitter with a photopeak at 81 keV and with a half life of 5 days.

A NaI crystal–photomultiplier tube–preamplifier–pulse-height-analyzer system is adjusted to count the Xe^{133} photopeak. Rise in Xe^{133} activity with time in the charcoal trap is recorded during the anneal. In order to calculate fractional release, the total Xe^{133} initially in the specimen must be known, so the specimen is later melted, the total Xe^{133} is adsorbed on the same trap, and its activity is recorded. Every postirradiation anneal run (i.e., every specimen) yields a single point in Fig. 23.

B. Preparation, Analysis, and Handling of the Uranium Carbide Specimens

The uranium monocarbide specimens were obtained from Battelle Memorial Institute. After arrival at this Laboratory, specimens were stored in vacuum desiccators, and were not exposed to air except for periods of the order of several minutes during transfers.

The following specifications were supplied by Battelle Memorial Institute.[D1]

"Metallographic examination of all the material sent was typical of the hyperstoichiometric uranium carbide microstructure" [Stoichiometric UC contains 4.80 w/o carbon].

"Examples of structure of the uranium carbide material are shown in Figures 1, 2, and 3. Figure 1 is the microstructure of Casting 12 from which ten specimens were machined. This material contains 5.07 w/o carbon and has a somewhat equiaxed grain structure (grains appearing approximately 40 to 60 microns in diameter). Figure 2 is the microstructure of Casting 6 from which only four specimens were machined. Other portions of this casting were found to be unsound by radiographic examination and were discarded. This material contains 5.09 w/o carbon and, like Casting 12, its grain structure is somewhat equiaxed (80 microns in diameter). Figure 3 shows the microstructure of Casting 23. Here, instead of equiaxed grains, large radially oriented columnar grains dominate. Actually, the internal structure of most of the material we have sent you consists of columnar grains such as is shown in this photomicrograph.

"All specimens came from castings which were melted in an inert atmosphere by carbon electrode arc methods and were then drop-cast into 1/4-inch diameter graphite molds. A single batch of uranium with the following impurity analyses was used in the preparation of the carbides.

"Element	Content (ppm)	Element	Content (ppm)
Al	15-40	Ni	20-30
B	0.1	P	40
Be	0.2	Pb	2
Cd	0.5	V	5
Cu	5-10	Si	30-300
Cr	5-20	Zn	10
Fe	80-120	Ca	5-20
Mg	5	Ba	5
Mn	5	In	5
Mo	20	Au	5

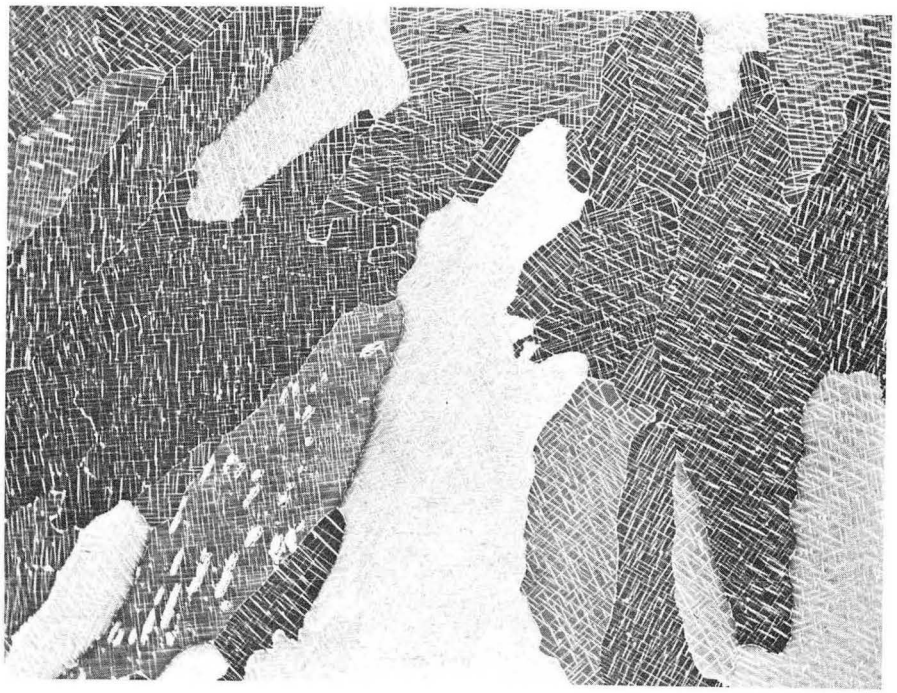

ZN-3584

Fig. 1. Microstructure of Casting 12, as cast. (Courtesy Battelle Memorial Institute)

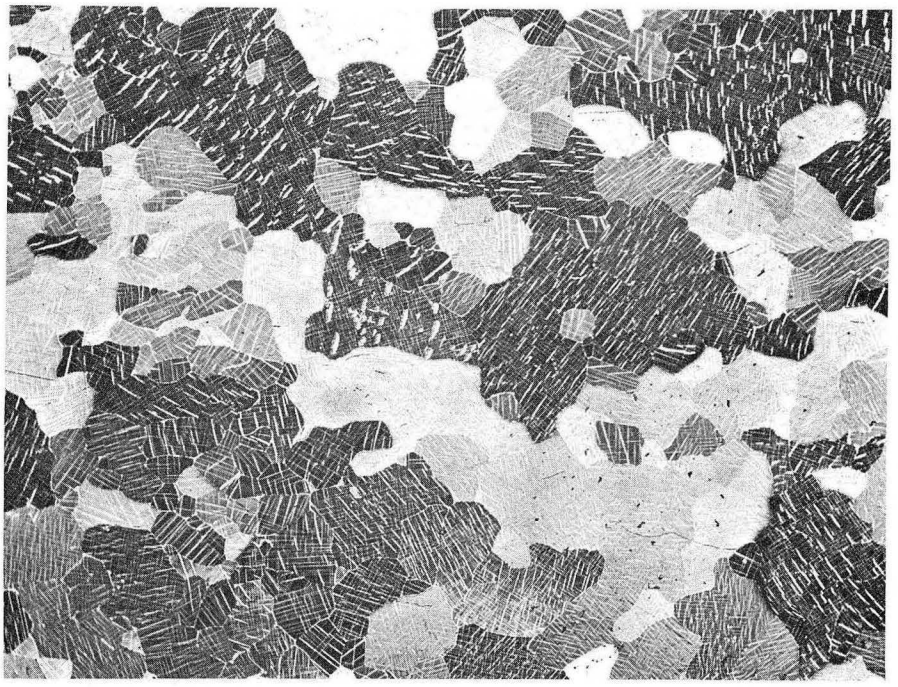

ZN-3585

Fig. 2. Microstructure of Casting 6, as cast. (Courtesy Battelle Memorial Institute)

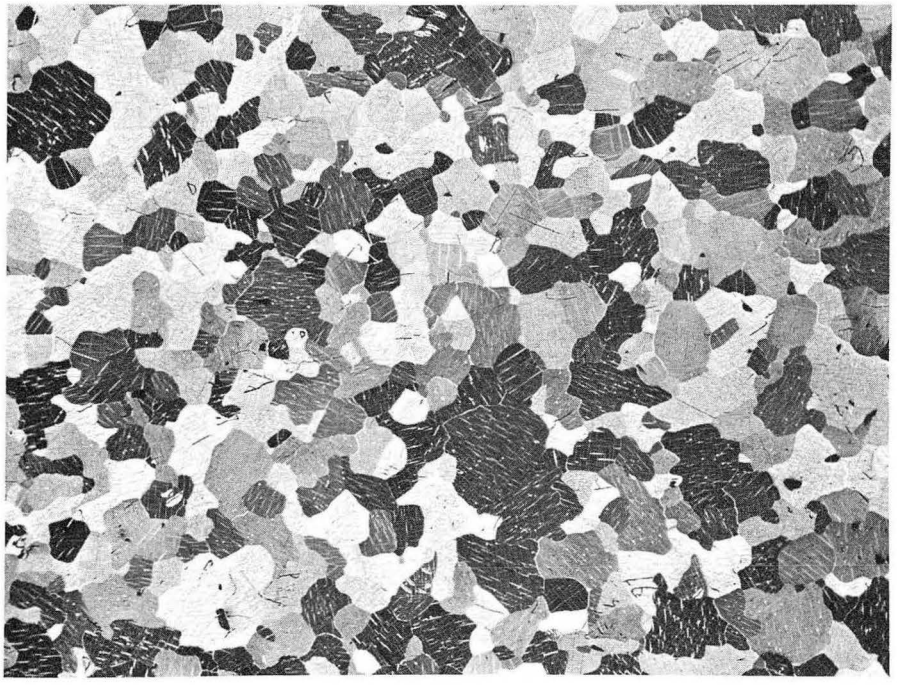

Fig. 3. Microstructure of Casting 23, as cast. (Courtesy Battelle Memorial Institute)

"Typical nitrogen, oxygen, and hydrogen analyses on uranium like that used are:

Element	Content (ppm)
N	200
O	150
H	5

"Castings were radiographed before and after machining. The initial radiographs were used as guides in machining; the latter ones were taken in two directions and were used in judging the soundness of the final specimens.

"In processing, the uranium carbide material was handled as little as possible and was exposed to the atmosphere for only very short periods of time. A light cutting oil, Sunoco Type 209-S, was used in machining. Immediately after machining, the specimens were thoroughly cleansed with acetone and were sealed in glass tubes with Drierite. In turn, these tubes were placed inside a disiccator also containing Drierite. After being initially sealed, the tubes were opened and resealed only one time (for several minutes) prior to their packaging for shipment -- for the removal of the chemical and metallographic samples and the scrap pieces.

"Specimens were machined from the castings in three operations. The first operation consisted of turning the castings on a lathe and milling (grinding) them with a 3/8-inch Norton diamond wheel (5D-150-5R grade) to the proper diameter. The second operation consisted of cutting the resulting cylinders into 0.5 centimeter lengths. A 1/32-inch Radiac 87468 cut-off wheel was used in this operation. Cutting was performed on the lathe by rotaing both the cut-off wheel and the cylinders (in opposite directions). In this manner, edge chipping was reduced to a minimum, although small protrusions of material resulted in the center of the fresh surfaces after cutting. These protrusions were subsequently removed in the final sizing operation by redressing the specimens and by again using the Radiac cut-off wheel.

"The number of specimens sent from each casting and the percentage carbon and the grain size of each of the castings are tabulated below. Carbon analyses were made utilizing a standard gravimeteric method, and grain sizes were determined by the Graff-Snyder intercept method. Of the 23 castings that were on hand at Battelle, 9 were discarded for such reasons as porosity, poor surface condition, or high carbon content.

Casting Number	Number of Samples Sent	w/o Carbon	Microstructure	Grain Size (*) (Microns)
1	9	5.13	Satisfactory	60 × 100
2	7	5.01	Satisfactory	50 × 80
4	6	5.15	Satisfactory	70 × 80
5	3	5.09	Satisfactory	90 × 90
6	4	5.09	Satisfactory	80 × 80
7	10	5.13	Satisfactory	100 × 110
9	8	5.13	Satisfactory	20 × 20
11	9	4.97	Satisfactory	50 × 440
12	10	5.07	Satisfactory	40 × 60
16	6	5.07	Satisfactory	80 × 100
20	9	5.14	Satisfactory	150 × 200
21	9	5.02	Satisfactory	60 × 70
22	5	5.12	Satisfactory	160 × 220
23	9	5.06	Satisfactory	120 × 580
Total	104			

(*) The grain size will vary with location along the length of the casting; see Figure 4 for metallographic specimens' locations.

"Precautions were taken during processing so that each specimen could be identified as to the casting and to the location within that casting from which it came. Figure 4 is a specimen identification chart which shows the exact location of each specimen in each casting."

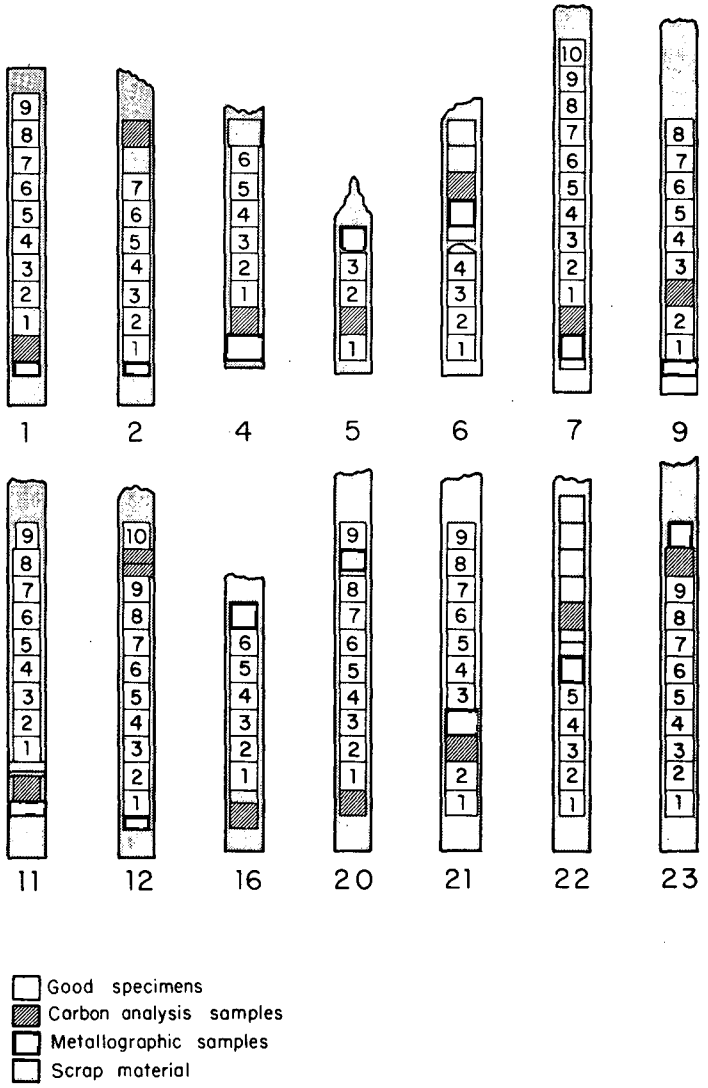

Fig. 4. Specimen-identification chart. (For example: the identification number of Specimen 2 of Casting 6 is 602; that of Specimen 9 of Casting 12 is 1209.) (Courtesy Battelle Memorial Institute)

C. Preanneal Activities

Specimens to be used in the experiment were taken from the vacuum desiccator and transferred into pyrex test tubes, one specimen to a tube. The tubes were evacuated, sealed, and sent to the Livermore pool-type reactor (LPTR) for neutron irradiation. Irradiation time of all specimens ranged between 2 and 10 minutes at a flux of 5×10^{12} n/cm^2-sec. By use of the Way and Wigner equation[W1] it was estimated that the combined beta and gamma activity of a single sample, three days after irradiation for 10 minutes at a thermal flux of 5×10^{12}n/cm^2-sec would be about 50 microcuries. After irradiation, specimens were cooled for at least 3 days before anneal.

When the specimen was to be transferred into the induction chamber (see Figs. 5, 6, and 7) the sealed pyrex tube was broken, the specimen transferred into the tungsten cup, and the top of the cup covered with a tungsten disc. The loaded cup, hanging on three tungsten wires, was inserted into the induction chamber from the top and positioned at the center of the induction coil, and the chamber was closed and evacuated with the auxiliary roughing pump. From the time it was removed from the vacuum desiccator until it was put into the induction chamber, the specimen was exposed to laboratory atmosphere for about 2 minutes during transfer to the pyrex tube, and about 3 minutes during transfer to the tungsten cup and positioning of the cup, or a total of about 5 minutes. A specimen was transferred into the induction chamber immediately after the preceding specimen had been removed at the end of its anneal.

While the auxiliary roughing pump was evacuating the induction chamber, a heater was inserted into the second trap and the charcoal was heated up to about 250°C. After the charcoal reached 250°C, the induction chamber roughing valve was closed and the induction chamber high-vacuum valve was opened. This last step usually took place at about 9:00 or 10:00 p. m. and the system was left overnight this way. At about 7:00 a. m. the heater was removed from second trap, and the trap was cooled with air and then filled with liquid nitrogen. At this point

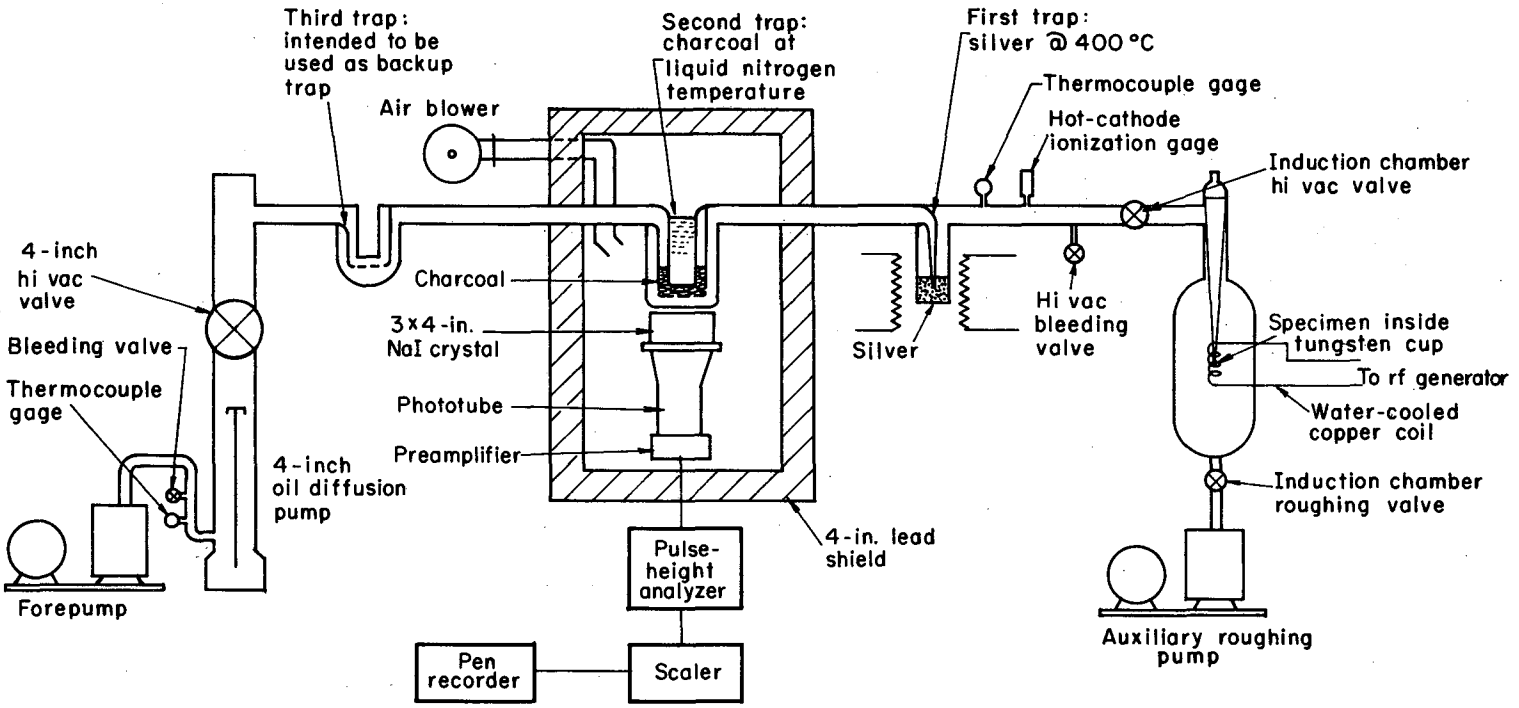

Fig. 5. Schematic arrangement of the postirradiation anneal apparatus.

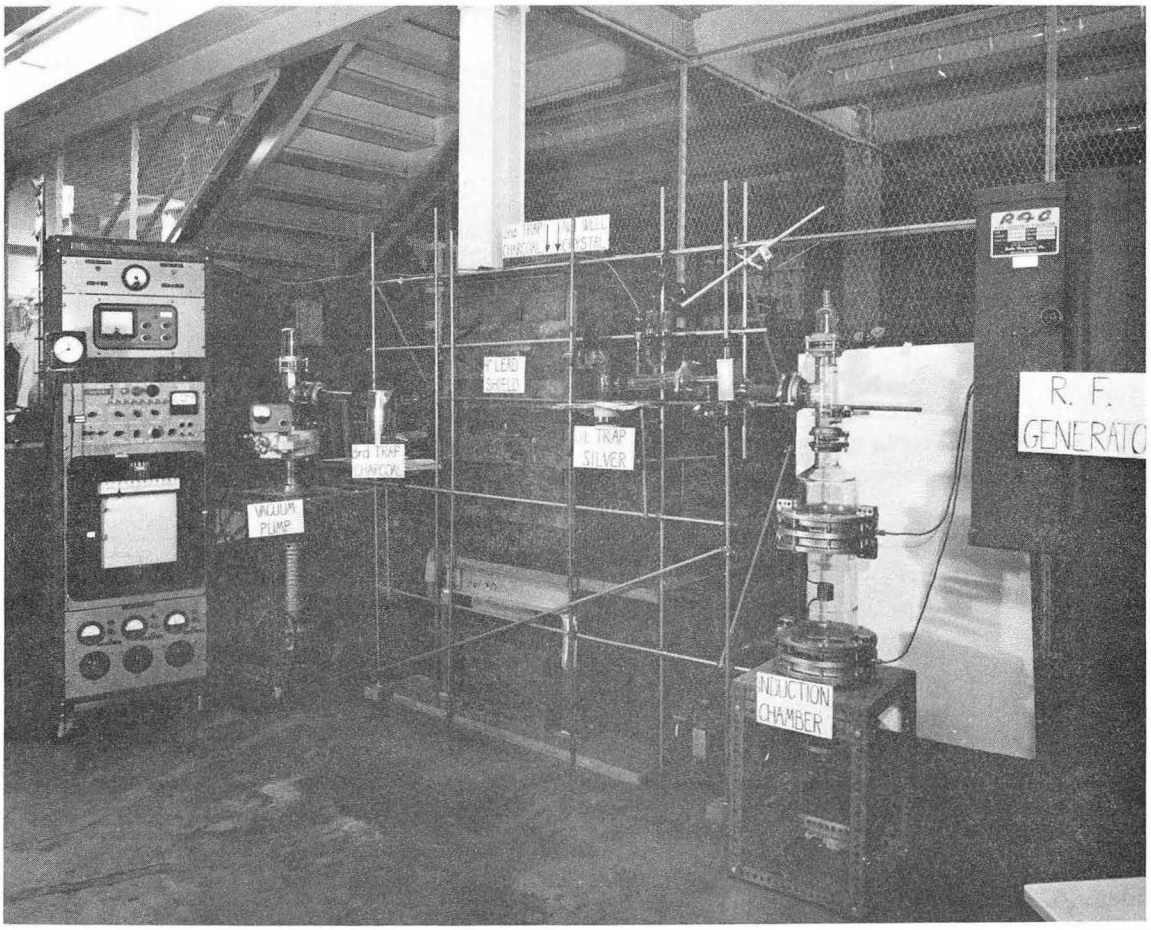

ZN-3589

Fig. 6. The postirradiation anneal apparatus.

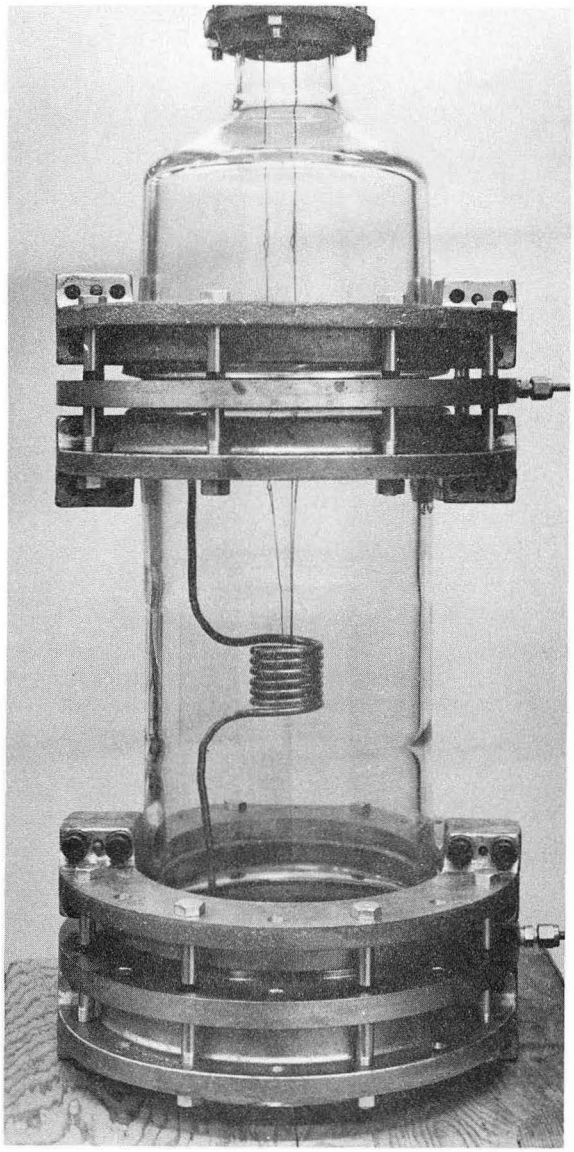

ZN-3590

Fig. 7. The induction chamber.

the pressure at the location of the ionization gage was between 10^{-4} and 2×10^{-4} torr. A 200-second background count was taken and the apparatus was ready for starting the anneal.

D. The Postirradiation Anneal and Meltdown of Specimens

After rf power was turned on, it took about a minute to adjust power to give the required tungsten temperature and about one more minute for the specimen to reach this temperature. Two minutes after rf power was turned on, a clock was turned on and counting of the Xe^{133} accumulating in the charcoal trap was begun at this point. In the first few seconds after rf power was turned on, the pressure of the system would rise as high as 5×10^{-4} torr in the low-temperature anneals and 2×10^{-3} torr in the high-temperature anneals. This pressure rise was due to degassing of the tungsten cup, the specimen, and the glass walls of the induction chamber, and about 10 to 20 minutes was required for restoration of the low pressure of 2×10^{-4} torr. In a few cases of high-temperature anneals in which pressure rose in excess of 5×10^{-3} torr it was found that the alternating induced field was intense enough to cause breakdown of the gas, which was evident as a blue glow of the whole induction chamber. To prevent possible breakage of the chamber, pressures in excess of 2×10^{-3} torr were avoided thereafter. For this reason, the backup trap was not filled with charcoal, so that pumping speed could be kept as high as possible.

An optical pyrometer was used to read the temperature of the surface of the tungsten cup. The true temperatures of this surface were obtained from the pyrometer temperatures[Pl] by using emissivities of tungsten as reported in reference G3. It was assumed that a specimen inside the cup was at the true temperature of the surface. This assumption was verified experimentally at several temperatures by direct observation of the specimen through a small hole in the tungsten cup. Drift of the rf output caused slow changes in temperature that amounted to 5 to 10°C in a period of 2 to 3 hours, so power was readjusted about every two hours.

Data were recorded in the first two columns of a data sheet of the type shown in Fig. 8. Count rates were computed and corrected for decay on the same sheet.

In several cases release was relatively high in the first few hours, so that the amount of gas released later was very small compared with that already accumulated in the trap. In order to avoid poor statistics in these cases, the charcoal trap was degassed for 10 minutes at 250°C (the specimen was kept at temperature), then was filled with liquid nitrogen and counting was started again from background level. This was done with specimen 203 (see Fig. 8).

Anneals lasted for about 12 hours. Specimens 1201 and 1206, the only exceptions, were annealed for only 5 hours. After rf power was turned off, a specimen was allowed to cool down for about an hour before the induction chamber was opened to atmosphere. At about 9:00 or 10:00 p. m. the annealed specimen was removed from the induction chamber and a new specimen was inserted, and the preanneal activities described in Section C were started.

The annealed specimens were stored in a separate vacuum desiccator for about 30 to 50 days after irradiation, then one by one were inserted again into the induction chamber and melted. This month or more of delay was to give the total Xe^{133} in the specimen enough time to decay, so that count rates at meltdown would be kept below the saturation count-rate of the scaler, which is about 1500 cps. The beginning of melting of the specimen was indicated by a large step increase in the activity at the charcoal; this step increase was observed at a pyrometer temperature of about 2200°C. Power was maintained at this temperature for about 5 to 10 minutes until the count rate leveled off, then power was increased to give a pyrometer temperature of about 2250 °C, which was maintained for about 3 minutes to make sure that the whole specimen melted. In most of the cases this increase did not affect the count rate. In a few cases, however, some more Xe^{133} showed up. In these few cases, an additional increase of about 50°C was applied. After it was made sure that increase in

NAME Date 08090740 Nº 96

SUBJECT 203 @ 1600°C Bkgrnd 3.2 cps Total 15200 cps

Relative Time t' sec.	Cum. Count x256	Time difference $\Delta t'$ sec	Count rate n'' cps	Count r. less bkg. n' cps	Mean time $t = t' + \frac{\Delta t'}{2}$ sec.	Correct for decay $e^{t/656640}$	Corrected count rate n cps	$\sqrt{\text{Time}}$ $\sqrt{t}$ $\sqrt{\text{sec}}$
98	10	98	26.1	22.9	49	1000	22.9	7.0
223	30	125	40.9	37.7	161	1000	37.7	12.7
374	60	151	50.8	47.6	299	1000	47.6	17.3
633	120	259	59.4	56.2	504	1001	56.3	22.5
948	200	315	65.1	61.9	791	1001	62.0	28.1
1316	300	368	69.6	66.4	1132	1002	66.5	33.7
2007	500	691	74.2	71.0	1662	1003	71.2	40.8
2667	700	660	77.7	74.5	2337	1004	74.8	48.4
3311	900	644	79.3	76.1	2989	1005	76.5	54.6
4254	1200	943	81.4	78.2	3783	1006	78.7	61.6
5185	1500	931	82.5	79.3	4720	1007	79.9	68.8
6110	1800	925	83.1	79.9	5648	1009	80.6	75.2
7030	2100	920	83.5	80.3	6570	1010	81.1	81.1
9500	000							
9890	5	390	3.29	0.09	9695	1015	0.09	98.4
10574	15	684	3.75	0.55	10232	1016	0.56	101.1
11977	40	1403	4.56	1.36	11276	1017	1.38	106.2
13455	70	1478	5.20	2.00	12716	1019	2.04	112.5
14741	100	1306	5.88	2.68	14108	1022	2.74	118.8
16716	150	1955	6.55	3.35	15739	1024	3.43	125.2
16820	000							
18600	50	1780	7.20	4.00	17710	1027	4.11	133.0
20215	100	1615	7.93	4.73	19408	1030	4.87	139.2
21675	150	1460	8.77	5.57	20945	1032	5.75	145.0
23048	200	1373	9.33	6.13	22362	1034	6.34	149.2
23100	000							
25655	100	2555	10.03	6.85	24378	1038	7.11	156.0
28035	200	2380	10.75	7.57	26845	1042	7.90	163.8
30275	300	2240	11.42	8.22	29155	1045	8.59	170.8
30320	000							
32455	100	2135	12.0	8.8	31488	1049	9.23	177.5
34438	200	1983	12.9	9.7	33447	1052	10.20	183.3
36325	300	1887	13.6	10.4	35482	1055	10.97	188.5
						over		

MUB-1439

Fig. 8. A data sheet for the postirradiation anneal experiment (Specimen 203).

temperature did not affect the count rate, rf power was turned off and the count rate was recorded.

E. Efficiency of the Charcoal Trap

At the meltdown of specimen 906 the silver trap was replaced by a charcoal trap. During the meltdown and for a period of 1 hour after meltdown, the second charcoal trap was continuously monitored. Count rate stayed at background level (2.9 counts/sec). The standard deviation for the 500-sec final counting period is 38.6 counts. As a second step, the first trap was degassed and Xe^{133} collected on the second trap. The 500-sec counting period yielded 73,000 counts. Therefore, the leakage through the first trap is smaller than $38.6/73000 \approx 5.3 \cdot 10^{-4}$.

F. Counting Technique

The instrumentation used for counting is schematically shown in Fig. 5. The photomultiplier tube and the 4×3-in. NaI crystal were assembled in an integral unit, type 16 MBW 12/A, by Harshaw Chemical Co. The recording pulse-height analyzer used incorporated a binary scaler in it and an output to a pen recorder. G2

The "window" (gate) of the pulse-height analyzer was set on photopeak of Xe^{133} at 81 keV. In order to achieve (a) as high count rate as possible, and (b) stability against drift of the photopeak, a relatively wide window of 20 volts was used; this was calculated to cover the energy range between 60 and 100 keV.

A reference Xe^{133} source, obtained from Oak Ridge National Laboratory, was used to reposition the window between runs. Figure 9 shows the spectrums of the Xe^{133}-adsorbing trap and of the reference source. The four sharp pulses seen there are built into the scanning system and are used as reference marks in positioning the window. Drift of the photopeak during the 12 hours of the anneal was hardly noticeable.

The pen recorder was used mainly in running energy spectrums and in repositioning the window. During the anneal it was used only

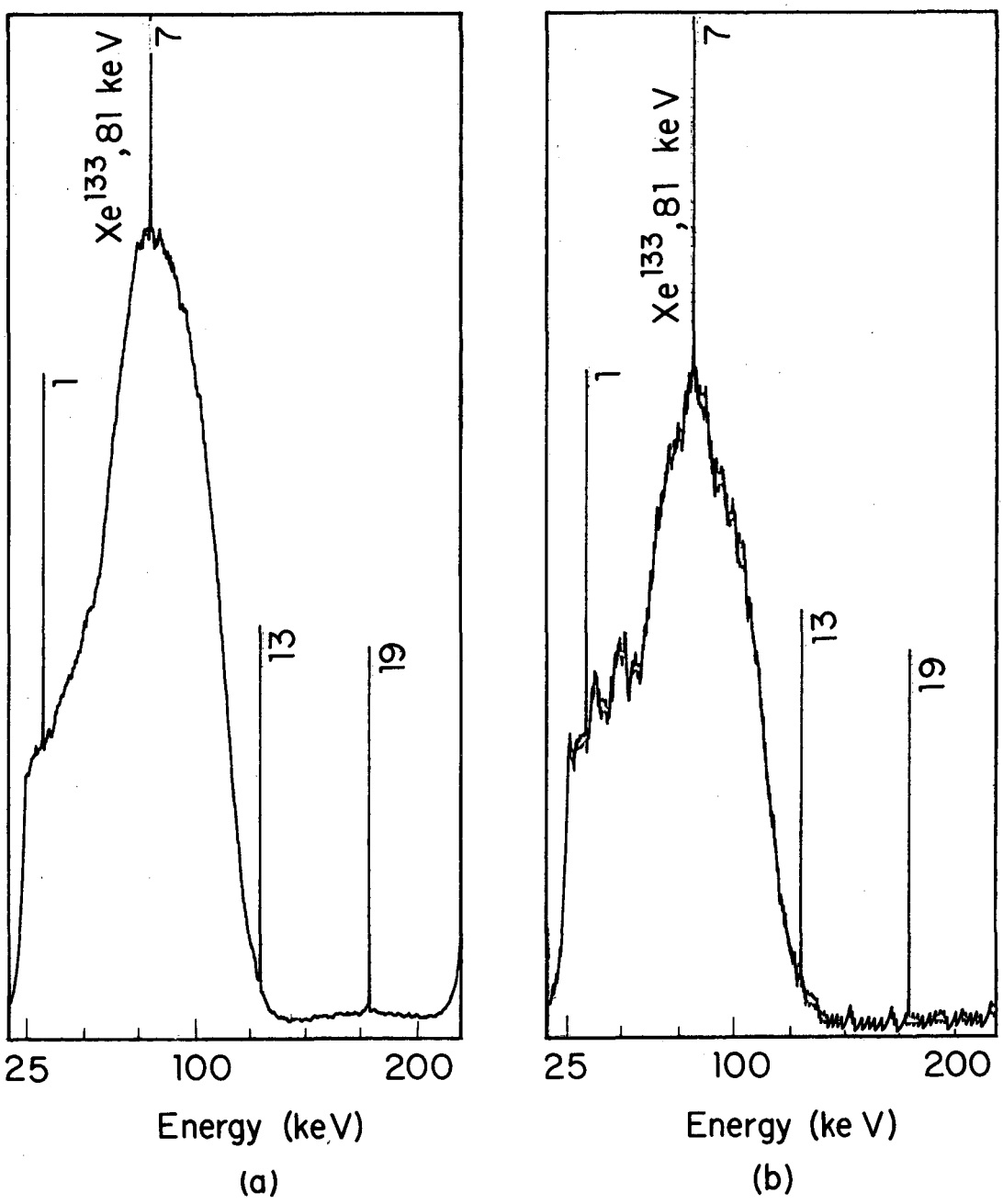

Fig. 9. Gamma energy spectra, at 0 to 220 keV, of (a) charcoal trap at the end of an anneal, (b) reference Xe^{133} source.

as an aid in following the release, and its trace was not used in the final analysis.

The internal dimensions of the 4-in. lead shield were 22×22 in. and it was 29 in. high (a similar shield is described in reference H1). A constant air stream was forced on the detector to keep it from getting too cold because of the liquid nitrogen or too warm during the degassing of the trap. Background outside the lead shield with an irradiated specimen in the induction chamber was about 100 counts/sec; inside the shield it was only 3 counts/sec. With this low background it was possible to measure release rates of the order of 10 counts/sec with exceedingly good statistics. For example, if we have 10 counts/sec from Xe^{133} and we count for 500 seconds, a fractional deviation (standard deviation in fraction of total count) is obtained,

$$\text{F. D.} = \sqrt{(3 + 13)\ 500}\ /(13 \times 500) = 0.0126,$$

or only 1.26%.

The effectiveness of the silver trap at 400° C is demonstrated in Fig. 10, which shows that only trace quantities of Te^{132} (77 h, 0.23 MeV) and I^{131} (8.1 days, 0.36 MeV) are present (Fig. 10a). Whereas in earlier runs a less dense silver trap was used at 300° C, the photopeak of Te^{132} appeared at that time to be almost as high as the Xe^{133} peak, although very little I^{131} was observed (Fig. 10b). This contamination from Te^{132} increased background at the Xe^{133} photopeak to about 20 counts/sec in the earlier runs. Ba^{140}, which was observed in similar experiments,[G1] was never observed in this experiment.

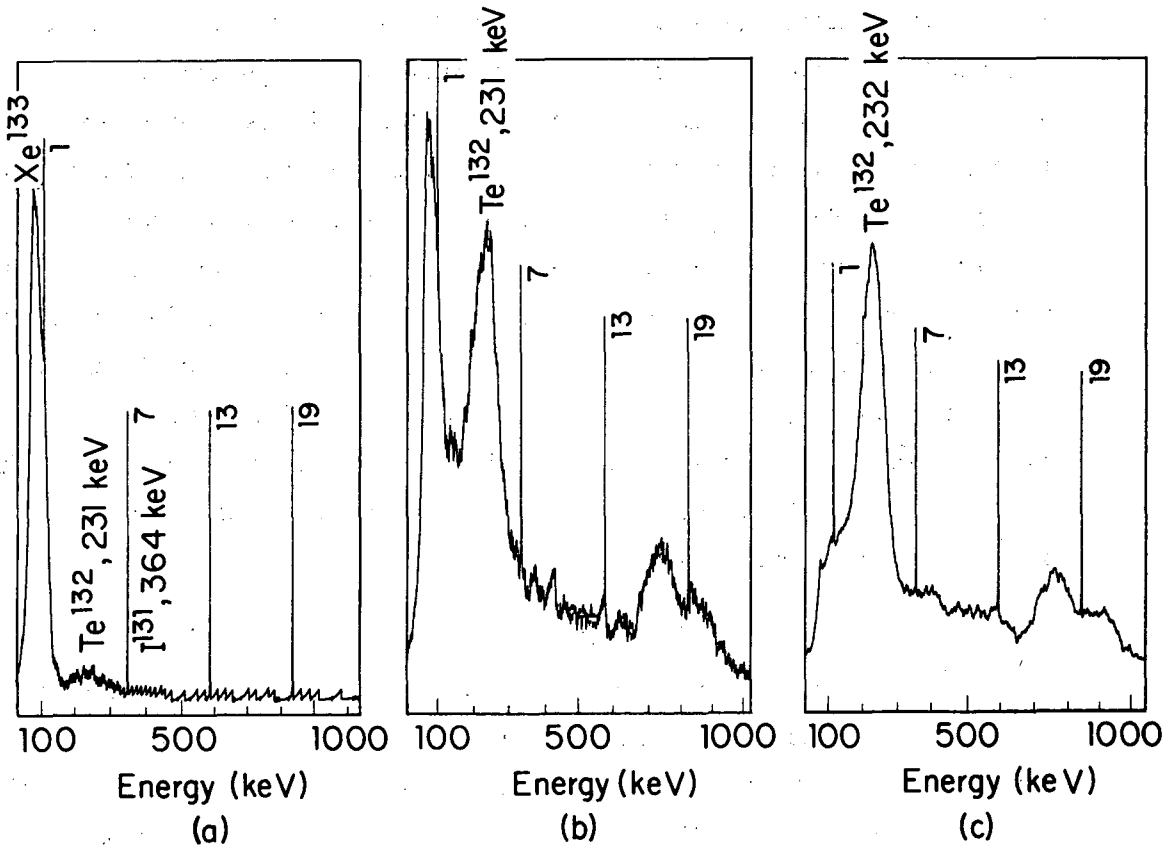

Fig. 10. Gamma energy spectra of charcoal and silver traps, 0 to 1000 keV (a) charcoal trap at the end of an anneal (b) charcoal trap at the end of an anneal in which a poor silver trap was used (c) silver trap.

III. ANALYSIS

A. Physical Model

The uranium carbide specimens are right cylinders of 0.5×0.5 cm. At the start of the anneal, Xe^{133} produced by fission during irradiation (see Sec. C) prior to the anneal is uniformly distributed throughout the specimen except for a depleted layer one recoil range thick next to the surface (Appendix A). It is assumed that the irradiation was at a temperature low enough so diffusion did not occur during irradiation. During the anneal some Xe^{133} is released from the specimen by the process of diffusion. It is assumed that the specimen is homogeneous (i. e., D is independent of location) and isotropic (i. e., D is independent of direction), and that the surface area through which Xe^{133} is released is identical with the external surface area of the specimen (i. e., no cracks or pores). This model does not take into account any possible effect of enhanced diffusion through grain boundaries.

B. Analytical Approach

For the sake of clarity the simpler case in which effect of recoil is neglected is formulated here. Then a correction function is used by which the diffusion coefficient D_{nr} obtained in this simpler analysis has to be multiplied in order to obtain the correct D.

The concentration C at any time t after start of the anneal is given by

$$
\begin{aligned}
&C_t = D_{nr}\left(C_{rr} + \frac{1}{r} C_r + C_{zz}\right), && \text{for } 0 \leq r < a, \quad -a < z < a, \quad 0 < t, \\
&C(r, z, 0) = C_0, && \text{for } 0 \leq r < a, \quad -a < z < a, \\
&C(r, \pm a, t) = 0, && \text{for } 0 \leq r \leq a, \quad 0 \leq t, \\
&C(a, z, t) = 0, && \text{for } -a \leq z \leq a, \quad 0 \leq t.
\end{aligned}
\qquad \text{(III-1)}
$$

The cumulative fractional release f is defined as

$$f(t) = \int_0^a r\,dr \int_{-a}^{a} dz \left[C(r, z, 0) - C(r, z, t)\right] \Big/ \int_0^a r\,dr \int_{-a}^{a} dz\, C(r, z, 0), \tag{III-2}$$

and is calculated from Eqs. (III-1) to be[J1]

$$f \approx \frac{6}{\sqrt{\pi}} \frac{(D_{nr}t)^{1/2}}{a}, \qquad \text{for } \frac{D_{nr}t}{a^2} < 0.01. \tag{III-3}$$

From this one has

$$D_{nr} \approx \frac{\pi}{36} \left[f_{\sqrt{t}}\, a\right]^2, \qquad \text{for } \frac{D_{nr}t}{a^2} < 0.01, \tag{III-4}$$

where

$$f_{\sqrt{t}} = df/d\sqrt{t}\ .$$

Now the model that takes into account the effect of recoil is formulated in Appendix B-3. In Appendix C is shown

$$D = M(\theta)\, D_{nr}, \tag{III-5}$$

where $\theta = \mu/2\sqrt{Dt}$, and $M(\theta)$ (Fig. 11) is a function of D. Hence D may be calculated by a trial-and-error procedure (Sec. D).

C. Application and Validity of the Model

The validity of Eqs. (III-4) and (III-5) is restricted to $Dt/a^2 < 0.01$,[J1] which is equivalent to $f < 0.3$. The largest release observed in this experiment (not considering porous or defective specimens) was from specimen 206; it amounted to $f \approx 0.0078$. Hence the experimental results are within the range of validity of the calculations.

The measured fractional release is a sum of two components: the initial large release, which is irrelevant to the diffusion process; and the diffusion component, which satisfies Eq. (I-5). The large initial release takes place during the first hour, and since the measured release is cumulative, it gives a constant contribution superimposed on the diffusion component. Therefore the magnitude of the measured fractional release can not be used. However, the rate of

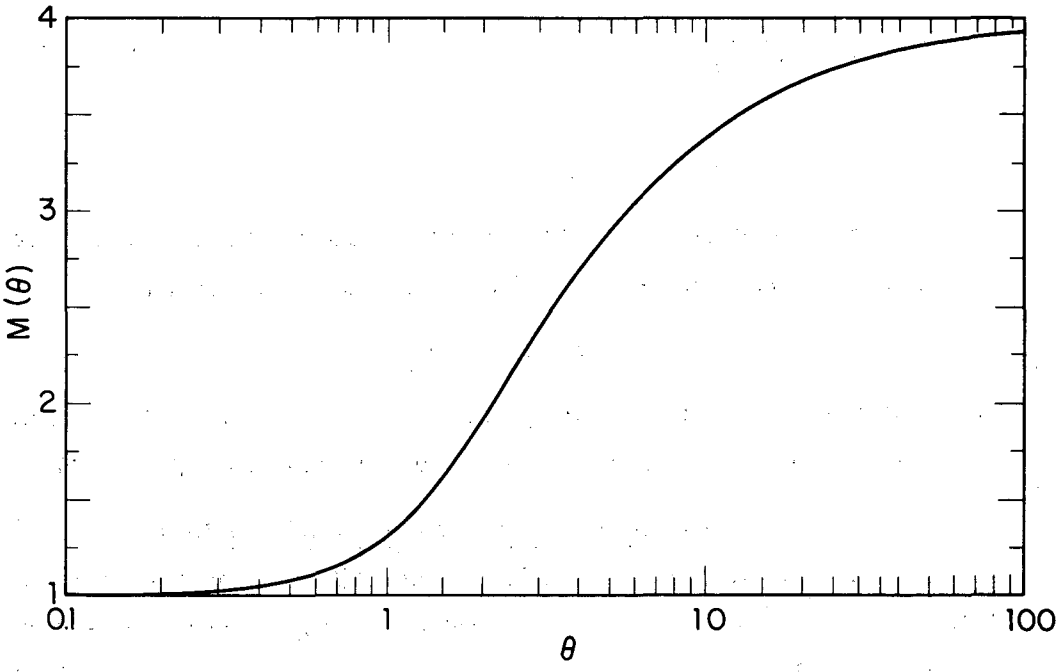

Fig. 11. The recoil correction function for the diffusion coefficient, cylinder height/diameter = 1

$$M = D/D_{nr} = \left[2/\left(1 + \frac{\sqrt{\pi}}{2}\,\frac{\text{erf}\ \theta}{\theta}\right)\right]^2$$

$$\theta = \mu/(2\sqrt{Dt})$$

increase of the measured fractional release with time is completely characterized by the diffusion component. The experimental results of each run are handled on a data sheet like the one shown in Fig. 8, and from this sheet a "release curve" like the one shown in Fig. 12 is plotted. The value of $f_{\sqrt{t}}(t)$ obtained from the slope of the release curve is substituted into Eq. (III-4), from which D is calculated in Section D by a trial-and-error procedure. The calculated value of D depends somewhat on the choice of $\sqrt{t}$ at which $f_{\sqrt{t}}$ is measured, as is subsequently demonstrated in Fig. 12. This discrepancy is an indication of some deviation from the assumed mathematical model, but the discrepancy in D is smaller than the actual spread in the results (Fig. 23) and is ignored throughout the analysis. A value of $t^{1/2} = 150\ \text{sec}^{1/2}$ seemed to be in a region far enough from the effect of initial release, without being too close to the end of the curve, so that slope could be established there most conveniently. Unless data were poor in this region $f_{\sqrt{t}}$ was determined at $\sqrt{t} = 150\ \text{sec}^{1/2}$.

In correcting for the decay of Xe^{133} a simple decay law characterized by a half life of 5.27 d was used.

Xe^{133} is a member of the mass-133 fission chain[B4]

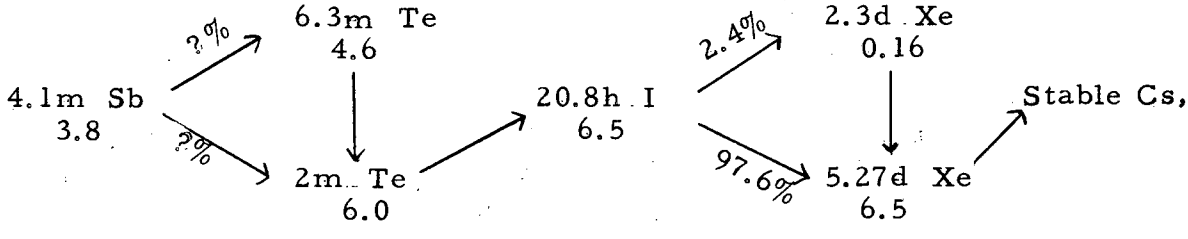

where the half life is given to the left of the isotope, and the fission yield in % is given below the half life. One day after irradiation the chain practically degenerates into

$$_{53}I^{133} \xrightarrow{20.8\,h} {}_{54}Xe^{133} \xrightarrow{5.27\,d} \text{stable Cs.}^{133}$$

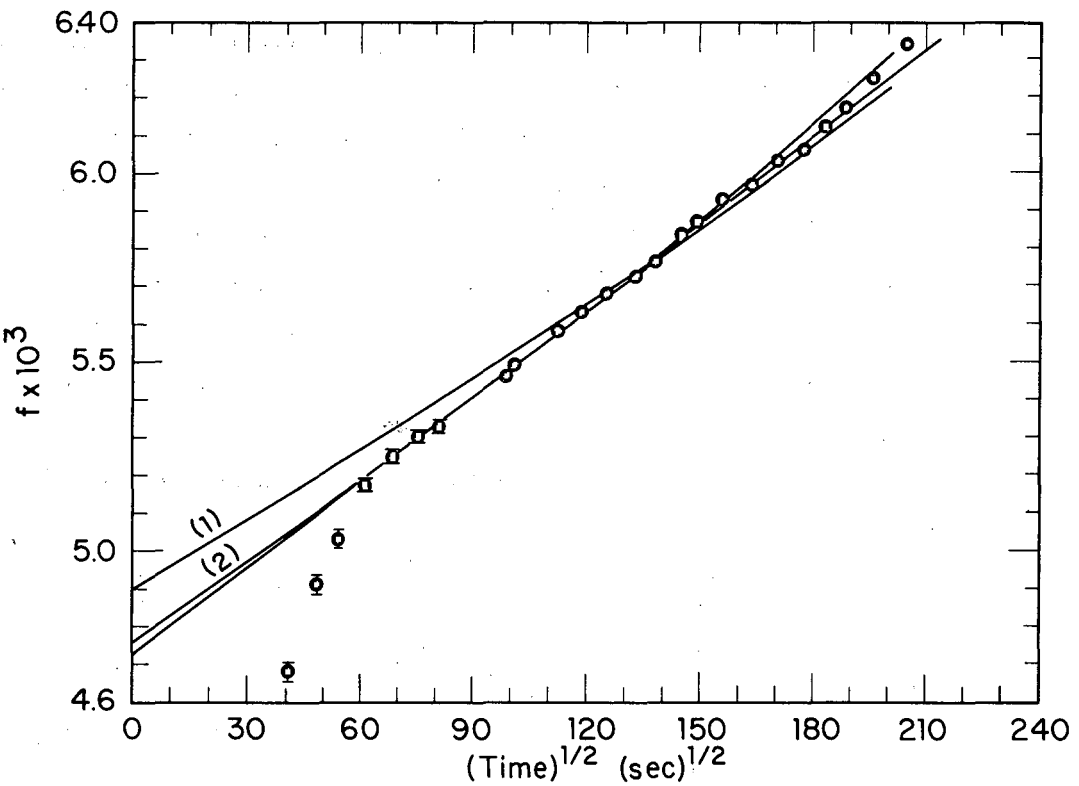

Fig. 12. Fractional release from Specimen 203, and theoretical fits.
(1): Predicted from $D = 5.5 \times 10^{-13}$ (calculated at $t^{1/2} = 200$ sec$^{1/2}$).
(2): Predicted from $D = 7.3 \times 10^{-13}$ (calculated at $t^{1/2} = 100$ sec$^{1/2}$).

At the fourth day the deviation of net Xe^{133} decay from the simple decay of 5.27 d half life, is 10%. Since three cooling days or more were allowed after irradiation, neglecting the effect of 20.8-h I^{133} is justified.

D. Calculation of D

Given $f_{\sqrt{t}}$ (= slope of release curve) at $\sqrt{t}$ one calculates D_{nr} from Eq. (III-4). This D_{nr} is used to obtain a first approximation for $\theta = \theta_1$, $M(\theta) = M(\theta_1)$ is determined from Fig. 11, and, by using Eq. (III-5), $D_1 = M(\theta_1)\, D_{nr}$ is obtained. Then D_1 is used in a completely identical manner to obtain D_2, and so on. The set D_1, D_2, D_3, $\cdots$, D_n formed in this way converges quickly, and beyond D_4 there is no change in the first two significant figures.

Results of these calculations are given in Table I.

Table I. Calculations of diffusion coefficient

Run No.	Specimen	Temp (°C)	$\sqrt{t}$ ($sec^{1/2}$)	$f_{\sqrt{t}}$ $\times 10^{-6}$	D_{nr} (cm^2/sec)	D (cm^2/sec)	$10^4/T$ $(°K)^{-1}$
1	1201	1900	100	200	2.2×10^{-10}	2.2×10^{-10}	4.61
2	1206	1900	100	18.7	1.9×10^{-12}	3.0×10^{-12}	4.61
3	401	1400	150	2.9	4.6×10^{-14}	1.3×10^{-13}	5.98
4	402	1600	150	7.1	2.7×10^{-13}	5.6×10^{-13}	5.34
5	403	1800	150	14.5	1.1×10^{-12}	1.6×10^{-12}	4.83
6	404	2000	150	29.9	4.9×10^{-12}	5.6×10^{-12}	4.40
7	405	1600	150	6.7	2.4×10^{-13}	5.1×10^{-13}	5.34
8	406	1840	100	33.8	5.7×10^{-12}	7.2×10^{-12}	4.74
9	101	1430	180	5.2	1.5×10^{-13}	3.2×10^{-13}	5.88
10	102	1430	150	3.5	6.6×10^{-14}	1.8×10^{-13}	5.88
11	103	1637	150	6.7	2.5×10^{-13}	5.2×10^{-13}	5.24
12	104	1637	150	10.0	5.4×10^{-13}	9.5×10^{-13}	5.24
13	106	1840	150	16.7	1.5×10^{-12}	2.1×10^{-12}	4.74
14	108	2040	150	34.8	6.6×10^{-12}	7.4×10^{-12}	4.33
15	109	1630	150	5.0	1.5×10^{-13}	3.4×10^{-13}	5.26
16	1202	1900	150	21.7	2.5×10^{-12}	3.2×10^{-12}	4.61
17	1203	1430	180	105	6.0×10^{-11}	6.0×10^{-11}	5.88
18	1204	1700	150	12.5	7.2×10^{-13}	1.2×10^{-12}	5.07
19	201	1015	150	1.2	7.8×10^{-15}	2.7×10^{-14}	7.77
20	202	1217	45	10.7	6.2×10^{-13}	1.7×10^{-12}	6.72

Table I (continued)

Run No.	Specimen	Temp (°C)	$\sqrt{t}$ ($sec^{1/2}$)	$f\sqrt{t}$ $\times 10^{-6}$	D_{nr} (cm^2/sec)	D (cm^2/sec)	$10^4/T$ $(°K)^{-1}$
21	203	1600	150	7.9	3.4×10^{-13}	6.7×10^{-13}	5.35
22	204	1800	150	480	1.3×10^{-9}	1.3×10^{-9}	4.83
23	205	1420	170	4.1	9.1×10^{-14}	2.2×10^{-13}	5.90
24	206	2040	100	39	8.3×10^{-12}	1.0×10^{-11}	4.33
25	704	1000	80	0.77	3.2×10^{-15}	1.2×10^{-14}	7.85
26	904	1000	80	2.25	2.8×10^{-14}	1.0×10^{-13}	7.85
27	906	1000	100	0.52	1.5×10^{-15}	5.6×10^{-15}	7.85
28	907	1400	150	5	1.4×10^{-13}	3.2×10^{-13}	5.98
29	2303	1200	50	2.9	4.6×10^{-14}	1.7×10^{-13}	6.78
30	2306[a]	1000	50	0.135	9.9×10^{-17}	3.9×10^{-16}	7.85
31	2306[a, b]	1500	150	3.6	7.1×10^{-14}	1.9×10^{-13}	5.65
32	2308[a]	1700	150	9.7	5.1×10^{-13}	9.1×10^{-13}	5.07
33	2309[a]	1200	80	0.64	2.2×10^{-15}	8.5×10^{-15}	6.78
34	2102[a]	1200	60	0.65	2.3×10^{-15}	8.8×10^{-15}	6.78
35	2103[a]	1800	150	150	1.2×10^{-12}	1.8×10^{-12}	4.83

a. Annealed for 12 hours at 2000° C prior to irradiation.

b. Since release at run No. 30 was extremely low, specimen 2306 was reused at 1500° C.

IV. DISCUSSION

A. The Initial Release

In postirradiation anneals at the high temperature range (1400°C to 2000°C) a large release rate was observed during the first hour or so. This initial release (Fig. 12) amounts to about 0.1% of total Xe^{133} at 1400°C and about 1.0% of total Xe^{133} at 2000°C. The time it takes to end this initial release does not seem to depend on temperature, and is always about one hour. At the low-temperature anneals (1000°C to 1200°C) there were several runs with no large initial release (Fig. 13) and several with initial release as low as 0.01% and as high as 0.05%. In most of the low-temperature runs the slope of the release curve was found to be increasing with time. In some runs this continuous increase started in the first hour, making it difficult to determine the initial slope (specimen 2103, Fig. 13). In most of the cases, however, this increase started only after 3 to 4 hours, and initial slope could easily be determined (specimen 2309, Fig. 13). The increase over the initial slope was by a factor of 10 or more, and the release rate at the end of anneal was of the same order of magnitude as in the 1500°C to 1700°C range. It seems that some physical change in the specimen is responsible for both the large initial release at the high temperature and the continuous increase in slope at the low temperature. Figure 14 shows results of a 12-hour anneal at 1600°C. Acicular UC_2, present before the anneal, disappeared after the anneal. From the uranium-carbon constitutional diagram (Fig. 15) it seems that one or both of two reactions are possible: (a) transformation to UC + U_2C_3, (b) transformation to cubic UC. At the low termperature the first one is more probable. It is possible that the large initial release at high temperature and the continuous increase in slope at the low temperature are due to these transformations. It is also possible that surface contamination (see Sec. E) is responsible for the large initial release. However, it is difficult to see how surface contamination can be responsible for the continuous increase in slope at low temperatures.

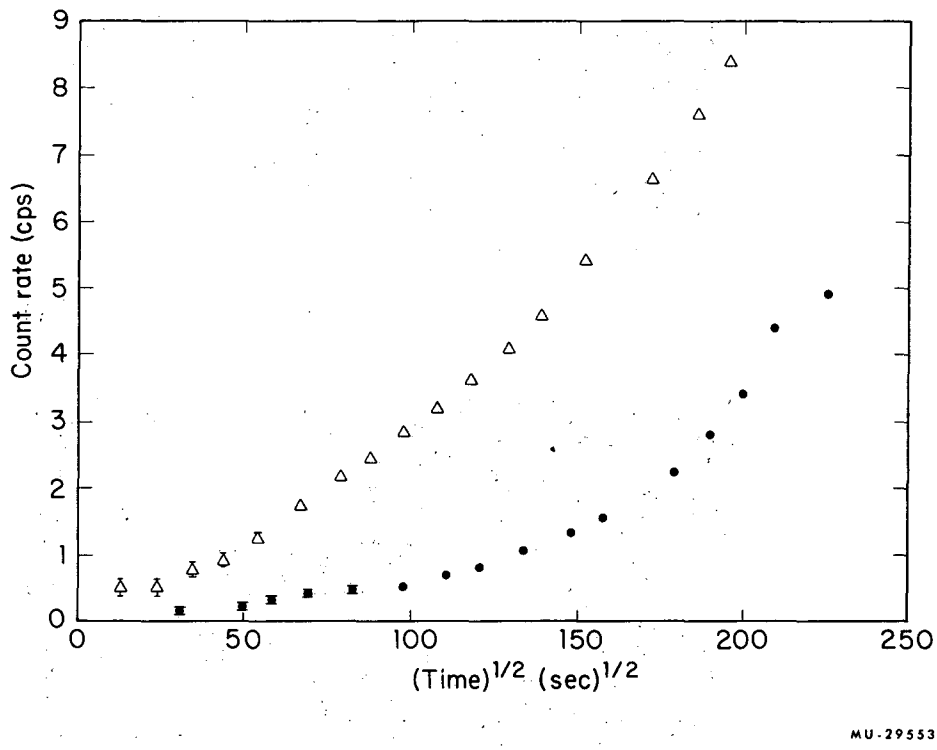

Fig. 13. Build-up of Xe^{133} in the charcoal trap during post-irradiation anneal at 1200 °C.
- O Specimen 2309 3.1 days after irradiation
- △ Specimen 2103 5.5 days after irradiation

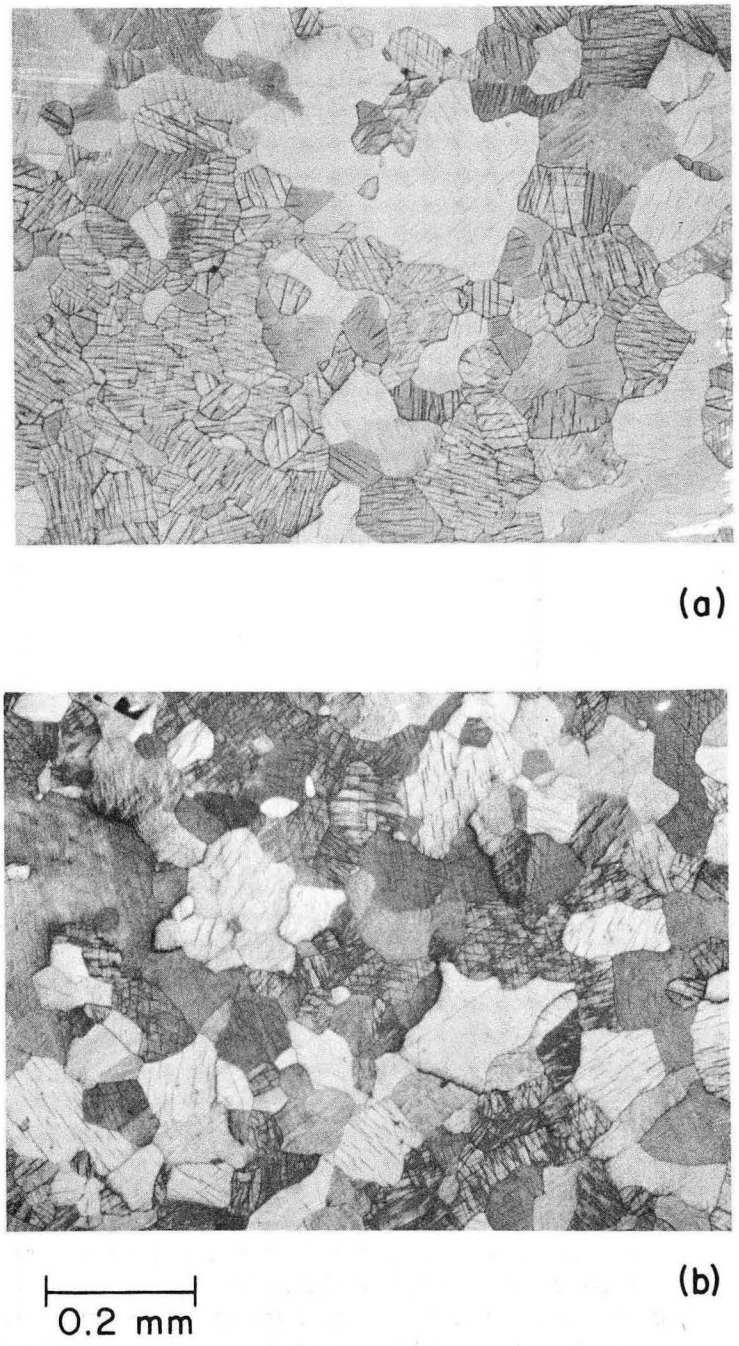

Fig. 14. Microstructure of Specimen 2101: (a) as cast, and (b) after 12 hours' anneal at 1600° C.

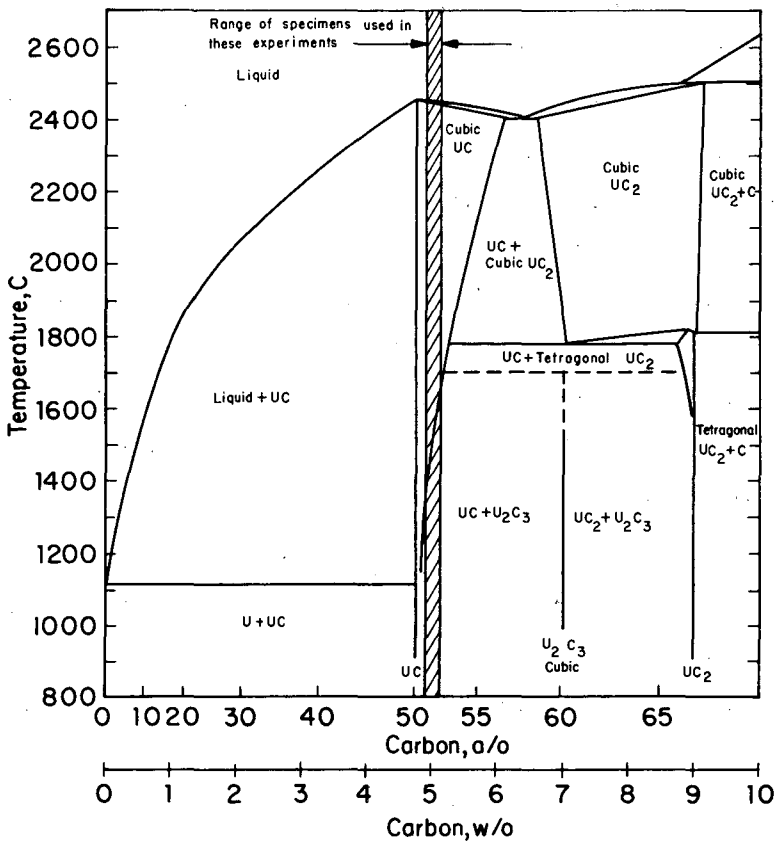

Fig. 15. Uranium-carbon constitutional diagram (from reference R2).
(Some changes in this diagram have been reported recently, in reference R1).

B. Increase in Apparent Diffusion Coefficient After a Long Anneal at 2040°C

Specimen 108 was annealed for 36 hours at 2040°C. An increase in slope of the plot of f vs $\sqrt{t}$ was observed after 12 hours; at the end of 36 hours, the slope was almost twice the initial slope. It is possible that evaporation of UC is responsible for this increase. From free-evaporation data (Fig. 16)[A1] a weight loss of 200 mg/cm^2/h would be predicted at 2040°C if the specimen were not surrounded by the hot tungsten cylinder. However, the small holes in the tungsten cup cover about 1/500 of the area seen by the specimen, so evaporation is about 0.4 mg/cm^2/h, or surface speed of 0.3 micron/h, or 11 microns per 36 hours. This corresponds to a volume decrease of about 1%, which calls for a fractional release of 1% (with no diffusion). The release during the 36-hour anneal of specimen 108 was about 1.3%. Therefore, it is very possible that the increase in slope was caused by evaporation.

C. Grain Growth

The extent of grain growth during 1 and 11 hours' anneal at 2000°C is shown in Figs. 17 and 18 respectively. During the first hour, average grain size increased by a factor of 5 to 7, and during the following 10 hours grains increased only by a factor of 2 to 3. No grain growth is observed after a 12-hour anneal at 1600°C (Fig. 14). On the basis of a theory of grain-boundary movement[K2] it is generally believed that lattice diffusion is not affected by grain growth occurring simultaneously with the diffusion. The high-temperature (2000°C) diffusion coefficients were measured in this experiment while grain growth was taking place. If diffusion were affected by grain growth, the high-temperature D should deviate from the straight-line fit of the low-temperature D. As shown in Fig. 23, this is not the case here. This observation offers experimental support to the above hypothesis.

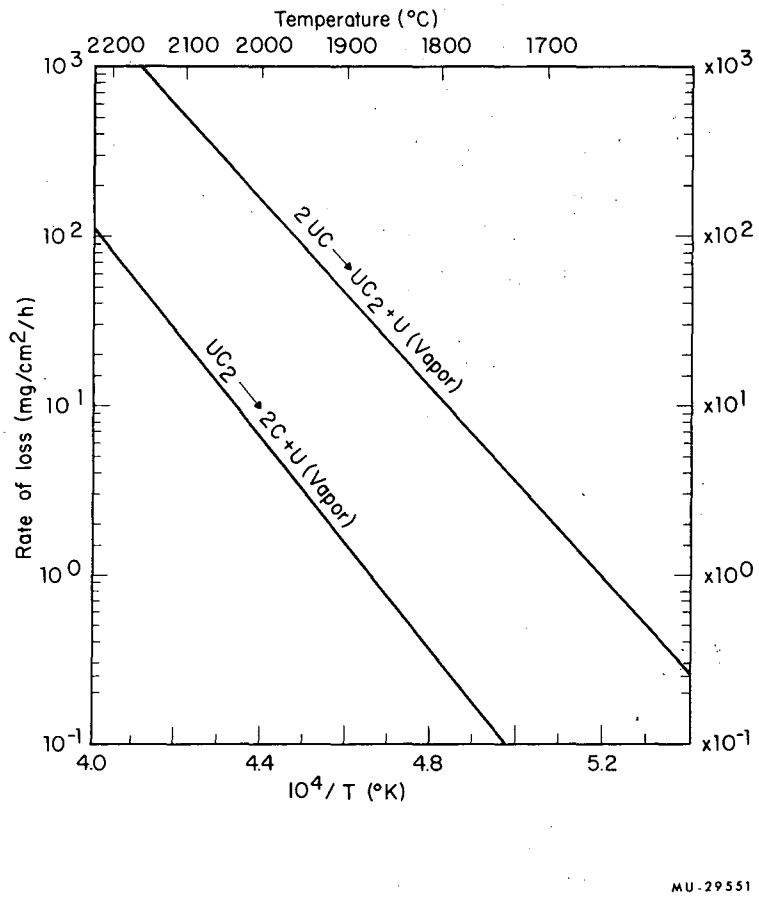

Fig. 16. Rate of weight loss (mg/cm^2/h) from UC [compacts], assuming free evaporation, as a function of temperature.

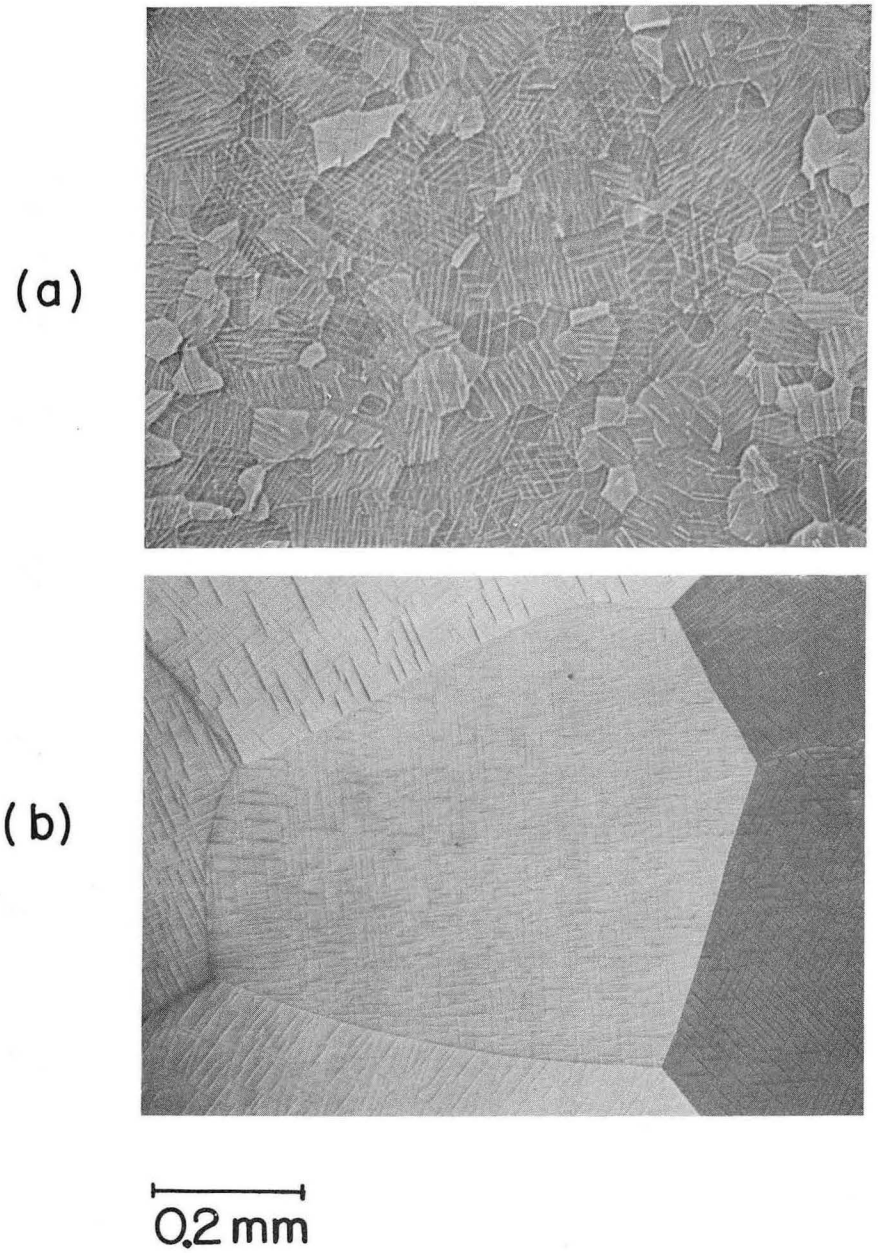

Fig. 17. Microstructure of Specimen 1601: (a) as cast, and (b) after 11 hours' anneal at 2000 °C.

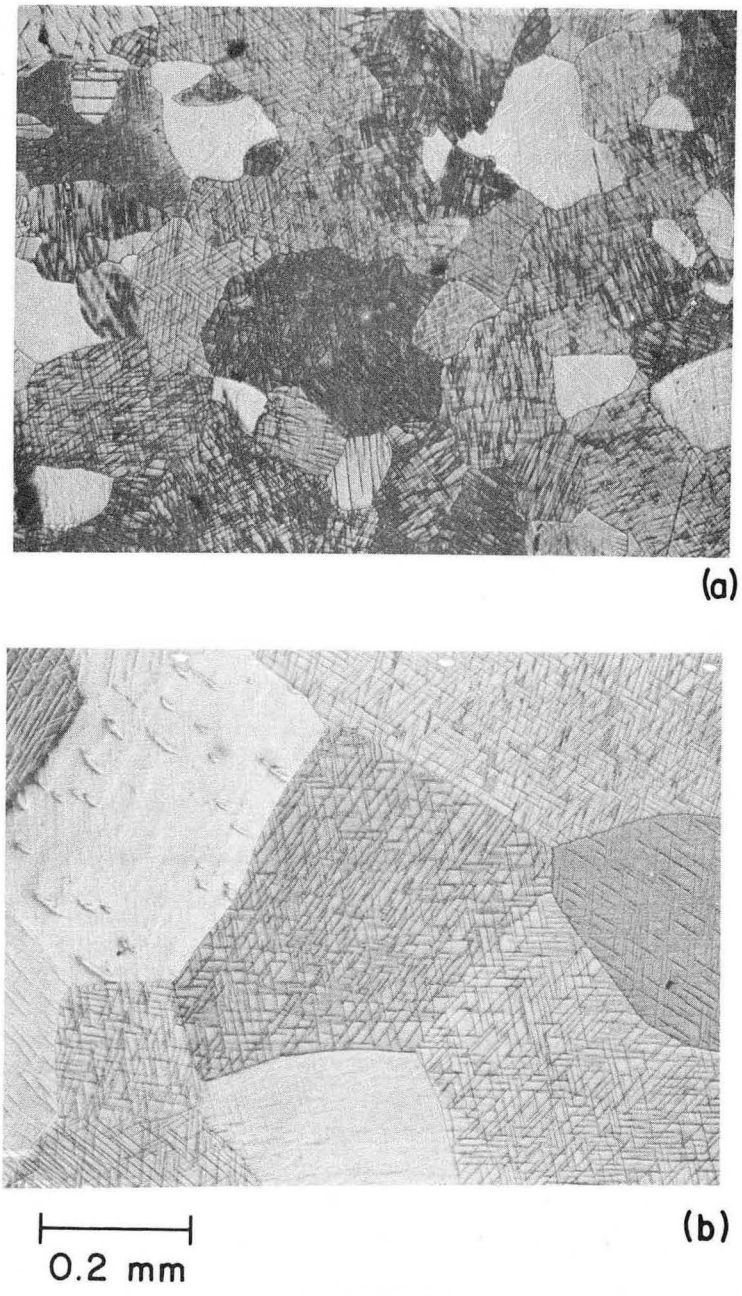

Fig. 18. Microstructure of Specimen 1606: (a) as cast, and (b) after 1 hour's anneal at 2000° C.

D. Effect of Grain Size on the Release

In the model used in the analysis, it is assumed that the cast cylinder behaves as a single crystal as far as diffusion is concerned. This is equivalent to assuming (a) that there are no internal surfaces (due to cracks, pores, etc.), and (b) that release via diffusion through grain boundaries is negligible compared with release via lattice diffusion. Among twelve metallographically examined specimens, the apparent diffusion coefficient of only one specimen (specimen 204) was considerably larger than expected (see Table I, Sec. III-D). Specimen 204 was also the only one among the twelve specimens that revealed some porosity in the metallographic examination. This circumstance offers partial support to assumption (a). In order to verify assumption (b) it is sufficient to show that the results are independent of grain size.

In Fig. 23, the solid circles represent specimens that were annealed for 12 hours at 2000°C prior to irradiation. These specimens developed grains as large as 700 to 1000 microns (shown in Fig. 19). The open circles represent specimens with grain size of 20 to 150 microns (specimens 203, 904, and 907 are shown in Fig. 20). The effect of grain size is not noticeable above 1500°C, whereas below 1400°C results are very strongly affected by grain size. Hence, assumption (b) is valid above 1500°C but breaks down below 1400°C.

This important result points out a fundamental difference between cast uranium monocarbide and sintered urania, since the rate of fractional release in the latter was found to be dependent on grain size, [B5] even above 1500°C.

The results of Lindner and Matzke indicate that variations of grain size should have no effect on fractional release rate at temperature below 1300°C, [L4] which is at variance with our results in this low temperature range.

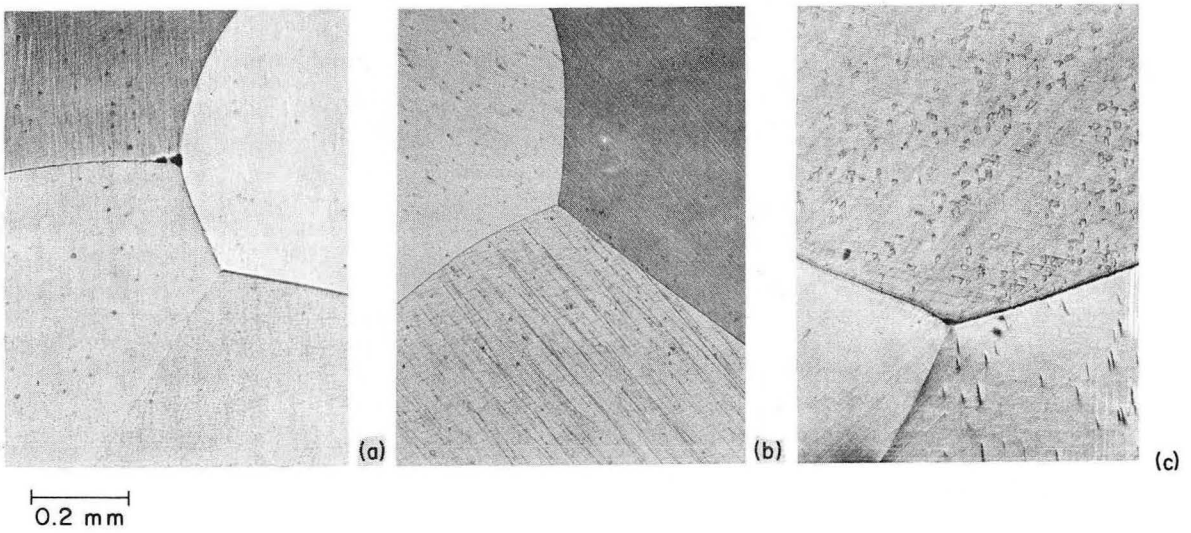

Fig. 19. Microstructures of three specimens after 12 hours' postirradiation anneal: (a) 2309, 1200 °C; (b) 2308, 1700 °C; (c) 2306, 1500 °C. All were annealed for 12 hours at 2000 °C prior to irradiation.

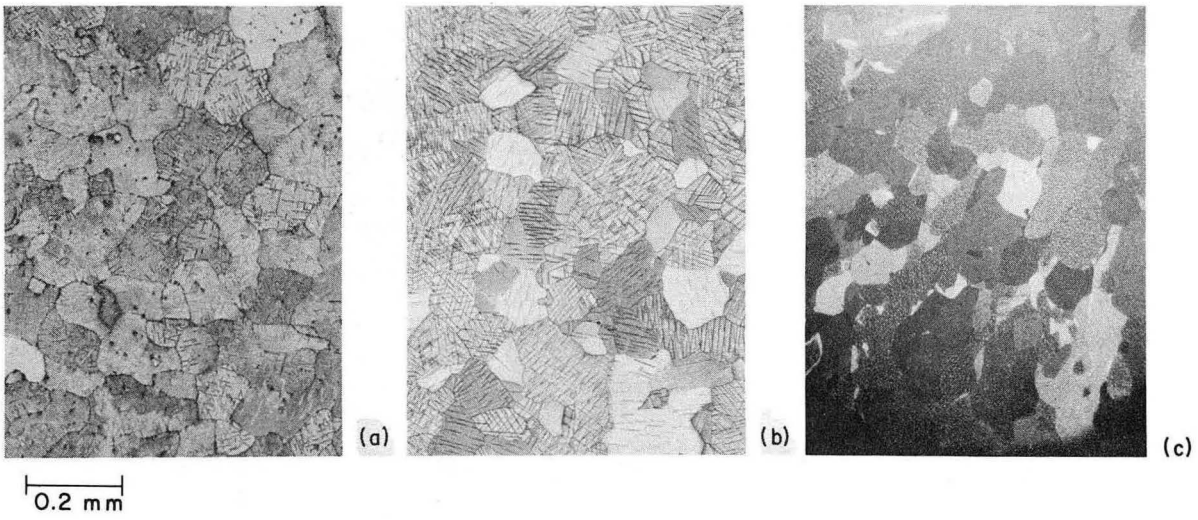

ZN-3580

Fig. 20. Microstructures of three specimens after 12 hours' postirradiation anneal: (a) 203, 1600 °C; (b) 904, 1000 °C; (c) 907, 1400 °C.

E. Surface Condition of Specimens

The specimens are assumed to have a smooth surface; since surfaces are not perfectly smooth, we are overestimating D. An underestimate by a factor of two in the surface area involes an overestimate by a factor of four in D. Because of porosity in specimen 204 (Fig. 21), the diffusion coefficient for this specimen appeared about 10^3 times as high as expected. This anomaly is probably due to porosity and, for it to be corrected, the surface area would have to be 31 times the apparent external surface area.

Specimen 1203 was irradiated and annealed once at 1400°C, yielding a reasonably low release (compared with other specimens with the same irradiation flux time). It was not melted and two months later was irradiated again. Between irradiation and anneal the specimen was exposed to atmosphere for eight days, then it was annealed and melted. The diffusion coefficient for this specimen was found to be 1500 times as large as expected. The effect of exposure to atmosphere on the surface of specimen 2003 is shown in Fig. 22; there is clearly an increase in the surface area. It is, of course, possible that the enhanced diffusion is also due to chemical changes in the grains. X-ray diffraction on the surface shown in Fig. 22 revealed no compound other than UC. It is worth mentioning that an increase in the apparent diffusion coefficient upon oxidation was also observed in UO_2.[S2]

F. Bursts of Xenon-133

In four cases bursts of Xe^{133} were observed at anneals between 1200°C and 1700°C. In three cases the bursts amounted to about 10 to 25% of the total release. In one case, however, it was about 100% of the total release.

In all four cases, the bursts occurred after several hours of anneal. After the burst, diffusional release proceeded regularly. The burst phenomenon was not investigated any further because of the small number of occurrences in this experiment.

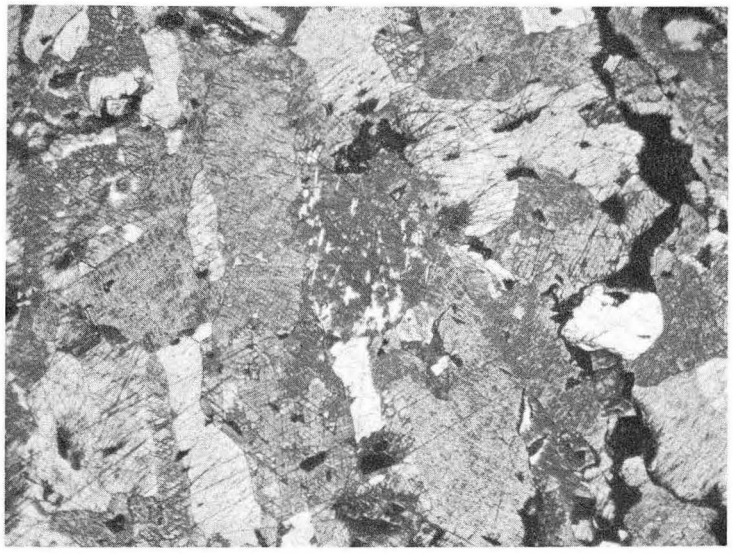

Fig. 21. Porosity in Specimen 204, as cast.

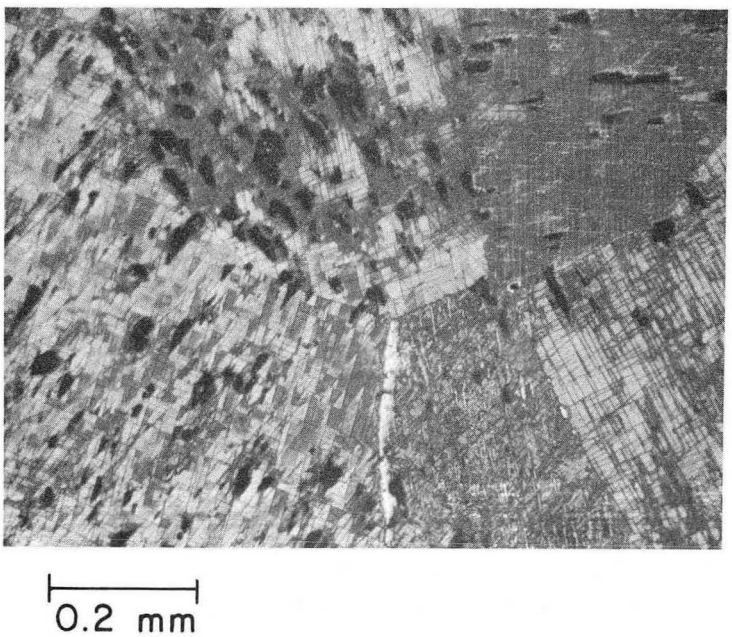

ZN-3581

Fig. 22. Porosity in Specimen 2003 caused by exposure to air (room temperature) for 14 days. The large grains were formed during 12 hours' anneal at 2000 °C, prior to exposure to air.

G. Precision of the Experimental Results

The straight line representing the data (Fig. 23) was calculated by minimizing the sum of the squares of the deviations.[V1] Data points for specimens with small grains below 1500°C and those for specimens 204, 1201 (not shown in Fig. 23), and 406 were rejected from the analysis. It was found that the data can be represented by

$$D = (1.17 \pm 0.16)\, 10^{-6} \exp\left[-\frac{54900 \pm 1200}{RT}\right], \qquad (IV-1)$$

where 0.16×10^{-6} cm^2/sec and 1200 cal/mole are equal to the standard deviations in D_0 and E respectively.

There are several possible sources of errors which may be the cause for the spread in the experimental results. The error in counting is easily evaluated (Sec. II-F), and the standard deviation in D due to this error is generally less than 4%. The error in temperature readings is 5 to 10°C (Sec. II-D), and the corresponding error in D is smaller than 10% at 1000°C and smaller than 5% at 2000°C.

The surface condition, both geometrical and chemical, is probably responsible for most of the scatter in the data. The released xenon atoms come from a relatively thin layer next to the surface. The thickness of this layer is approximately equal to $\frac{a}{2}f$. For example, in specimen 203 (Fig. 12) this layer is about 8 microns. Hence, any chemical contamination just several microns thick strongly affects the rate of release. The lower the anneal temperature the smaller $\frac{a}{2}f$ and the stronger the effect of surface contamination. At temperatures below 1400°C we have also the interference of phase transformation (discussed in Sec. A). The rate of transformation depends on the extra carbon content, the state of strain, and the UC_2 and U_2C_3 grain size. So, scatter in results below 1400°C may be due to these three properties in addition to surface condition.

H. Theoretical Fit of the Recoil Model to the Experimental Results

The recoil correction $M(\theta)$ is plotted in Fig. 11. With anneal times of 12 hours, the correction is practically equal to unity above 1800°C and to approximately 4 below 1400°C. The recoil model calls for a time dependence of the fractional release as shown in Fig. 27 (in the Appendix). We have assumed $\mu = 5$ microns, on the basis of recoil range data in UO_2.[B1] The release with no recoil correction is represented in Fig. 27 by the line $\mu = 0$. Two theoretical fits of the curve $\mu = 5$ to the experimental release of specimen 203 are shown in Fig. 12. The initial release of this specimen amounts to 4.7%, whereas the recoil release during irradiation amounts to 1.5%. Hence, the concentration profile after the initial release has occurred is possibly perturbed more by the initial release then by the effect of recoil. The low-temperature runs, in which initial release was exceedingly small, were not useful in testing the theoretical predictions because of the anomalous increase in slope of the plot of f vs $t^{1/2}$ (Fig. 13).

I. Comparison with the Results of Other Experiments

Data obtained by Lindner and Matzke[L4] and part of the data obtained by Auskern and Osawa[A2] are shown in Fig. 23. It is difficult at this time to explain the differences between these experimental results, but some possible explanations are given below.

Lindner and Matzke measured the release from polycrystalline particles of two sizes (0.02 and 0.25 mm) at the temperature range 800°C to 1300°C. In this temperature range one should expect release via grain-boundary diffusion as well as by lattice diffusion. It is possible that the release measured by Lindner and Matzke was via both types of diffusion, thereby yielding apparent diffusion coefficients larger than would be obtained for pure lattice diffusion.

Auskern and Osawa measured the release from UC powders (0.26 to 0.28 m^2/g) at the temperature range 1000°C to 1400°C. The

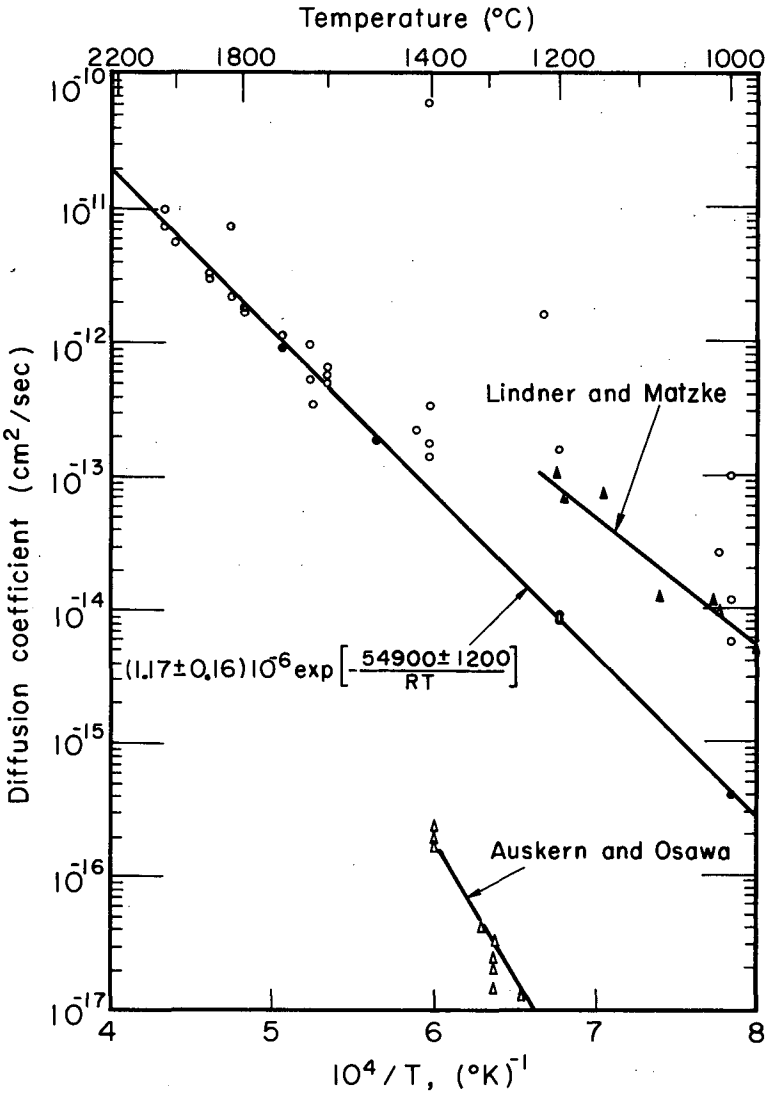

Fig. 23. The diffusion coefficient of Xe^{133} in UC.
- ● specimens with large grains, 700 to 1000 μ
- ○ specimens with small grains, 20 to 150 μ
- ▲ data obtained by Lindner and Mazke
- △ data obtained by Auskern and Yasutaka

experiment was of the multitemperature anneal type,[A2, L3] and anneal at each temperature lasted between 50 and 100 hours. As can be seen in Fig. 23, the results obtained by Auskern and Osawa are considerably lower than those obtained here. A possible reason for these low results is the effect of a variation in particle size, as is discussed in Appendix F.

J. Some Simple Theoretical Considerations

The general dependence of the diffusion coefficient on the lattice structure is reasonably well understood.[L1] In order to obtain a theoretical prediction of the magnitude of D for Xe^{133} in UC crystals one has to treat the thermal vibrations of the Xe^{133} atom in the UC lattice (fcc) and the vibrations of the lattice itself in some detail. Calculations of this type have been carried out in the relatively simple case of self-diffusion in copper.[H3] These calculations are extremely laborious and are not considered here.

A very simple model,[J2] which restricts us to a rather qualitative discussion, is considered here. The model is rather general and applies to lattice as well as grain-boundary type of diffusion through the various mechanisms (i.e., vacancy, interstitial, interchange, etc.). According to this model,

$$D = \frac{d^2 \nu}{3} \exp\left(-\frac{E}{RT}\right), \qquad \text{(IV-2)}$$

where d is the lattice spacing and ν is the frequency at which the diffusing atom (i.e., Xe^{133}) vibrates. E is equal to some average height of the potential barrier that the diffusing atom has to cross in order to change its position in the lattice (in vacancy-type diffusion, E also includes the energy it takes to make a vacancy).

Since a grain boundary may be considered as a region of high density of vacancies, we expect the potential barriers there to be lower relative to those in the interior. With lower potential barriers frequencies should be lower (for a harmonic oscillator, $\nu \propto (k/m)^{1/2}$, where k is the "Spring constant.") Let the superscripts L and G

represent lattice and grain-boundary type diffusion respectively, then

$$E^G < E^L ; \quad D_0{}^G < D_0{}^L . \tag{IV-3}$$

This qualitative observation is consistent with the various data scattered in the literature.[L1, S1]

The ratio of the release through grain-boundary diffusion to that through lattice diffusion is approximately

$$\frac{f^G}{f^L} \approx \frac{F^G}{F^L} \left(\frac{D_0{}^G}{D_0{}^L}\right)^{1/2} \exp\left(\frac{E^L - E^G}{2RT}\right), \tag{IV-4}$$

where F^G is the external surface area associated with grain boundaries and F^L is external surface area associated with the lattice. Equation (IV-4) is only approximately valid for very short times (i.e., $(D^L t)^{1/2}/a^L \ll 1$ and $(D^G t)^{1/2}/a^L \ll 1$, where a^L is a mean grain size). Let a^G be mean width of the grain boundary, then, assuming cubical grains, we have

$$\frac{F^G}{F^L} \approx \frac{4\, a^L (a^G/2)}{\left[a^L\right]^2} = \frac{2a^G}{a^L} \tag{IV-5}$$

and

$$\frac{f^G}{f^L} \approx \frac{2\, a^G}{a^L} \left(\frac{D_0{}^G}{D_0{}^L}\right)^{1/2} \exp\left(\frac{E^L - E^G}{2RT}\right) . \tag{IV-6}$$

From Eq. (IV-6) it is evident that release through lattice diffusion is the rate-controlling process at high temperature, whereas diffusion through grain boundaries controls at the low temperatures. This is demonstrated by the experimental results in Fig. 23 (small grains). Furthermore, according to Eq. (IV-6), the larger the grain size the lower the temperature at which the "break point" between the two processes should appear. This also is demonstrated by the results in Fig. 23.

V. CONCLUSIONS

The diffusion coefficient of Xe^{133} in cast specimens of uranium monocarbide was measured. The effect of grain size on the apparent diffusion was studied and it was found that there was little or no effect at temperatures above 1500°C, whereas at the temperature range 1000°C to 1200°C the effect was appreciable. The original cast material had relatively small grains ranging between 20 and 150 microns. The temperature dependence of the diffusion coefficient measured on this material can be approximated by

$$D = (1.17 \pm 0.16)\ 10^{-6} \exp\left[- \frac{54900 \pm 1200}{RT} \right],$$

valid for temperatures higher than 1500°C. The units of D are cm^2/sec and RT is given in cal/mole. With specimens that had large grains, about 700 to 1000 microns in size (solid circles in Fig. 23), the validity of the above equation is extended down to 1000°C. In other words, specimens with large enough grains behave like single crystals as far as diffusion is concerned.

A mathematical model that takes into account the effect of fission recoil on the diffusional release was developed. The fractional release predicted by this model is different from that predicted by the conventional nonrecoil model (i.e., Eq. I-4); the difference, however, was too fine to be demonstrated in this experiment. It is believed that upon elimination of the secondary release phenomena mentioned in part IV. A, B it should be possible to verify this model by showing that it offers a better fit to the experimental curve than the nonrecoil model.

Since the temperature range 1000°C to 1500°C is of primary importance in application to nuclear reactors, a basic investigation of the release and its dependence on grain size in this range seemed worth while. The phenomena of large initial release and continuous increase in slope of release curve at low temperatures (part IV. A) as well as at high temperatures after a long anneal (part IV. B) call for better understanding. An investigation of single crystals under close

mechanical and chemical control also seemed very worth while. Such an experiment may be of some help in understanding the reasons for the difference between the three sets of data in Fig. 23.

It will be advantageous to run a single specimen through several anneals, each at a different temperature, and obtain D vs T for that specimen. Since the fractional release depends on τ, it is possible in principle to accurately correct for the release in the preceding anneals.[L3] A practical method of analysis should be developed for this important procedure.

The apparatus used was found adequate, and is recommended for use in future experiments of this type with the four following improvements:

(a) Automation of the temperature control.

(b) Automation of refilling of the liquid nitrogen trap.

(c) Automation of the scaler readout.

(d) Replacement of the meltdown procedure for total gas release (which consumes a tungsten cup for each two meltdowns) by a "low"-temperature chemical reaction that can be carried out in a relatively inexpensive boat.

ACKNOWLEDGMENTS

I would like to take this opportunity to thank the many individuals who have made this work possible:

Professor Thomas H. Pigford, who initiated and supervised this work;

Dr. Donald R. Olander, for his kind interest and criticism;

Dr. Richard M. Fulrath, for some valuable ideas;

Mr. Leonel Stollar, for his kind help with problems of apparatus and design;

Mr. Steven Merril for his help in the runs;

Mr. Gerard F. Helfrich, of the Atomic Energy Commission, San Francisco Operations Office, for his continuous cooperation.

The work was done under the auspices of the U. S. Atomic Energy Commision.

Appendix A

THE EFFECT OF RECOIL ON THE DISTRIBUTION OF FISSION PRODUCTS

1. Statement of the Problem

A specimen of fissionable material is irradiated in a uniform neutron flux. The maximum temperature in the specimen is small enough so that thermal diffusion of fission products during irradiation may be neglected. It is desired to determine the distribution of fission products in the specimen at the end of irradiation. This distribution will serve as an initial condition in solving the diffusion problem of the anneal experiment.

For the sake of simplicity, let us follow a single fission product and denote it as the "tracer." The fact that a tracer atom is a member of a chain of nuclear transformations (e. g., isotope C, where $A \rightarrow B \rightarrow C \rightarrow D$) is irrelevant to the following treatment (because isotope C is found in the exact location where isotope A ended its recoil flight). The recoil range of the tracer atom (isotope C) refers to the range of the parent fission product of the chain (i. e., isotope A). The concentration of the tracer atoms refers to the concentration of the isotope being followed (i. e., isotope C).

If the fission recoil range of these tracer atoms were zero and the fission density were uniform throughout the specimen, the concentration of tracer atoms at the end of irradiation would be uniform. Diffusion is negligible at the temperature at which these specimens are irradiated. However, recoil range is finite, hence concentration of tracer atoms is uniform in regions more than one recoil range away from the surface, where the region within one recoil range from the surface is depleted of tracer atoms.

The spatial dependence of the tracer atom concentration will be derived for a slab and a sphere, assuming a single recoil range. It will be shown then that the spherical case reduces to the slab case when the recoil range is small compared with the radius of the sphere. The conditions under which we can approximate an infinite cylinder by

a slab will be determined. Finally, the case of variable recoil range will be treated.

2. Slab

In the case of practical interest the slab thickness 2a is large compared with the recoil range μ (see Fig. 24), therefore only one surface of the slab at $z = a$ needs to be treated. We assume that

(a) the tracer has a distinct recoil range μ,

(b) the fission density is uniform,

(c) the probability that a tracer atom will be emitted into an angle $d\Omega$ is equal to $d\Omega/4\pi$ and is independent of Ω.

The number of tracer atoms that end their recoil flight at a point z is proportional to the surface area of a spherical sector with radius μ centered at z, or

$$C(z) = A\, 2\pi\, \mu\, (\mu + a - z), \text{ for } (a - \mu) < z < a \quad . \tag{A-1}$$

The value of the constant A is to be determined from the boundary condition,

$$C(a - \mu) = C_0 \, . \tag{A-2}$$

Here $C(z)$ is the concentration--that is, tracer atoms per unit volume--in the external region $(a - \mu) < z < a$, and C_0 is the constant concentration in the internal region $0 < z < (a - \mu)$.

From Eqs. (A-1) and (A-2) we obtain

$$C(z) = (C_0/2\mu)\, (a + \mu - z), \text{ for } (a - \mu) < z < a. \tag{A-3}$$

Equation (A-3) gives $C(a) = C_0/2$, which is to be expected on physical grounds, since the plane at the surface ($z = a$) of the slab receives a contribution from only one side ($a > z$), while a plane in the internal region receives equal contributions from both sides.

3. Sphere

Using the same assumptions as in Section A. 2, we obtain for a sphere (see Fig. 25)

$$C(r) = B\, 2\pi\, \mu\, \left(\mu + \frac{a^2 - r^2 - \mu^2}{2r}\right), \text{ for } (a - \mu) < r < a, \tag{A-4}$$

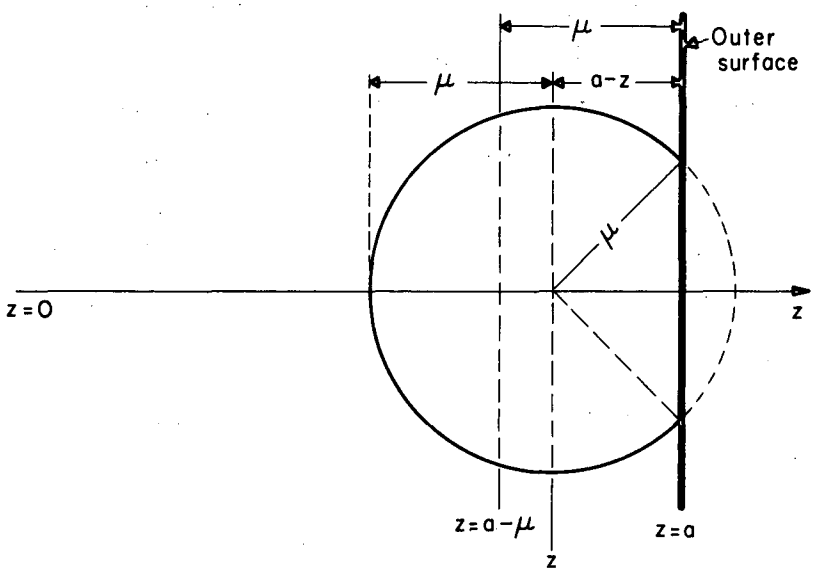

Fig. 24. Recoil in a plane geometry. Fission products with a recoil range μ that end their recoil flight at the point z come from fissions occurring on the surface of a spherical sector contained within the slab (solid line).

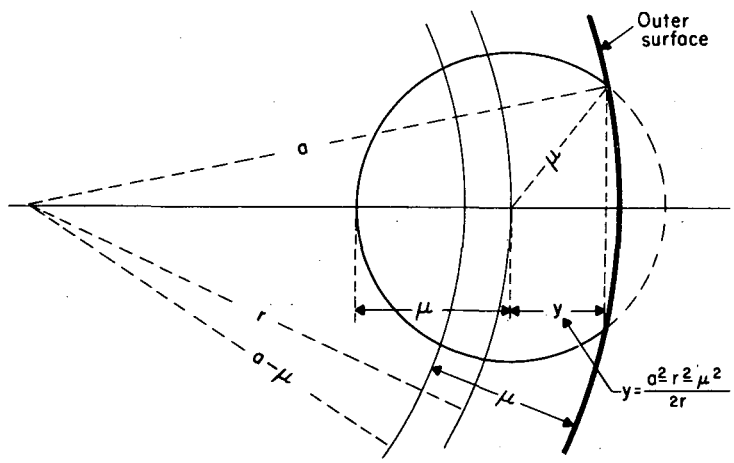

Fig. 25. Recoil in a spherical geometry. Fission products with a recoil range μ that end their recoil flight at the point r come from fissions occurring on the surface of a spherical sector contained within the sphere (solid line).

where a is the radius of the sphere and the constant B is determined from the condition

$$C(a - \mu) = C_0 ; \tag{A-5}$$

therefore,

$$C(r) = \frac{C_0}{2}\left[1 + \frac{1}{2\mu/a}\left(\frac{1 - (\mu/a)^2}{r/a} - \frac{r}{a}\right)\right], \text{for } (a - \mu) < r < a. \tag{A-6}$$

When μ/a is very small, C(r) can be approximated by C(z) of Eq. (A-3), as follows.

Let

$$\zeta = (a - r)/a \quad \text{or} \quad r/a = 1 - \zeta \ . \tag{A-7}$$

In the external region ζ is always smaller than μ/a; for $\mu/a \ll 1$, Eqs. (A-6) and (A-7) give

$$C(r) = C_0 \frac{1}{2}\left\{1 + \frac{1}{2\mu/a}\left\{\left(1 - \frac{\mu^2}{a^2}\right)(1 + \zeta + \zeta^2 + \cdots) - (1 - \zeta)\right\}\right\} \tag{A-8}$$

and if we neglect μ^2/a^2 and smaller terms with respect to unity, we obtain

$$C(r) \approx (C_0/2\mu)[a + \mu - r], \text{ for } (a - \mu) < r < a \ . \tag{A-9}$$

Equations (A-3) and (A-9) are identical in form.

4. Cylinder

Geometrical complications make it exceedingly difficult to obtain an exact solution for this configuration; hence a solution will be estimated. Since a cylindrical surface of radius a has less curvature than a spherical surface of the same radius, but more curvature than a flat surface, the cylindrical solution is expected to be bounded by the solutions of these two cases, i. e.,

$$C(\text{sphere}) < C(\text{cylinder}) < C(\text{slab}), \tag{A-10}$$

where the diameter of the sphere, 2a, is equal to the thickness of the slab.

From sections 2 and 3 we have, at the external region $a-\mu < z < a$,

$$C_{sl} \equiv C(\text{slab}) = \frac{C_0}{2\epsilon} (1 + \epsilon - x), \quad \text{for } (1 - \epsilon) < x < 1, \tag{A-11}$$

where $x = \frac{z}{a}$ and $\epsilon = \frac{\mu}{a}$, and

$$C_{sp} \equiv C(\text{sphere}) = \frac{C_0}{2}\left[1 + \frac{1}{2\epsilon}\left(\frac{1-\epsilon^2}{x} - x\right)\right], \quad \text{for } (1-\epsilon) < x < 1, \tag{A-12}$$

where $x = \frac{r}{a}$ and $\epsilon = \frac{\mu}{a}$.

Now, the error $\frac{C_0 |\delta|}{2}$ introduced when we approximate the concentration in the external region of a cylinder by that of a slab where

$$\frac{C_0}{2} |\delta| = [C(\text{slab}) - C(\text{cylinder})]_{max} \tag{A-13}$$

is bounded by the difference $C_{sl} - C_{sp}$ or

$$\frac{C_0}{2} |\delta| < \Delta(x) \equiv C_{sl} - C_{sp}, \tag{A-14}$$

and from Eqs. (A-11) and (A-12) we have

$$\Delta(x) = \frac{C_0}{2\epsilon}\left(1 - \frac{x}{2} - \frac{1-\epsilon^2}{2x}\right). \tag{A-15}$$

We want to find the maximum of $\Delta(x)$, therefore we set

$$0 = \frac{d\Delta}{dx} = \frac{C_0}{4\epsilon}\left(\frac{1-\epsilon^2}{x_m^2} - 1\right) \tag{A-16}$$

and

$$x_m = (1-\epsilon^2)^{1/2}, \tag{A-17}$$

so

$$\Delta_{max} = \frac{C_0}{2\epsilon}\left[1 - (1-\epsilon^2)^{1/2}\right]. \tag{A-18}$$

Since ϵ is small, we can expand the square root,

$$\Delta_{max} = \frac{C_0}{4} \epsilon \; ; \qquad \text{(A-19)}$$

therefore, in applying the flat-surface distribution of Eq. (A-8) to a cylinder we introduce an error δ, where

$$|\delta| < \frac{C_0 \epsilon/4}{C_0/2} = \frac{\epsilon}{2} = \frac{\mu}{2a} \; . \qquad \text{(A-20)}$$

In many practical cases $\mu << a$, and the error δ is indeed very small.

5. Variable Recoil Range

The total energy of a fission leading to a given pair of fragments and number of emitted neutrons is fixed, and is equal to the energy equivalent of the change in mass. This energy is divided into

(i) kinetic energy of fragments and neutrons,

(ii) excitation of fragments;

the sum of (i) and (ii) is equal to the fixed total energy. The amount of excitation (distortion) energy depends on the details of splitting, which is statistical in nature.[F1] Hence, the difference between total fission energy and excitation energy will be statistically distributed about some mean energy. Experimentally, the energy distribution of a particular fragment was found to be Gaussian, with a width at half height of about 8% for fission products of the light group.[C2]

It is outside the scope of this research to investigate the very complex range-energy dependence of heavy and highly ionizing particles such as fission fragments, so as a crude approximation we assume that the range is proportional to the initial speed.[B3] In this case, the variation in recoil range of most of the tracer atoms will be within 4% of the mean recoil range.

We shall now derive the distribution of tracer atoms in a slab (see Fig. 24), taking into account the variation in recoil range. Let P(w) be the probability that a tracer atom has a recoil range of length w, such that

$$\left.\begin{aligned} &\int_{\mu_{min}}^{\mu_{max}} dw\ P(w) = 1 \\ &\text{for } P(w) = 0, \quad \mu_{min} > w, \quad \mu_{max} < w. \\ &\qquad \neq 0, \quad \mu_{min} < w < \mu_{max}. \end{aligned}\right\} \tag{A-21}$$

Consider the concentration of the tracer atoms with a recoil range μ,

$$C_{\mu}(z) = C_{0\mu} - \Delta C_{\mu}(z), \tag{A-22}$$

where $C_{0\mu}$ is the concentration of tracer atoms with range μ in the internal region ($z < a - \mu$), and $\Delta C_{\mu}(z)$ can be calculated from Eq. (A-3),

$$\left.\begin{aligned} \Delta C_{\mu}(z) &= \frac{C_{0\mu}}{2}\left(1 - \frac{a - z}{\mu}\right), \quad \text{for } \mu > (a - z), \\ &= 0 \qquad\qquad\qquad\quad \text{for } \mu < (a - z). \end{aligned}\right\} \tag{A-23}$$

Since the probability P(w) is equal to the fraction of tracer atoms with range w about dw, we have

$$C_{0w} = P(w)\, C_0, \tag{A-24}$$

where C_0 is the concentration of tracer atoms of all possible ranges in the internal region $z < (a - \mu_{max})$.

To obtain concentration of tracer atoms anywhere in the slab we sum over all possible ranges,

$$C(z) = \int_{\mu_{min}}^{\mu_{max}} dw\ C_w(z), \tag{A-25}$$

where $C_w(z)$ is given by Eq. (A-22), also, using Eq. (A-24), we obtain

$$C(z) = \int_{\mu_{min}}^{\mu_{max}} dw\, P(w)\, C_0 - \int_{\mu_{min}}^{\mu_{max}} dw\, \Delta C_w(z) . \qquad \text{(A-26)}$$

Using Eqs. (A-21), (A-23), (A-24), and (A-26), we have

$$C(z) = C_0 - \frac{C_0}{2} \int_{h-z}^{\mu_{max}} dw\, P(w)\, (1 - \frac{a-z}{w})$$

$$= \frac{C_0}{2} \left[1 + (a - z)\, \frac{\bar{I}}{\mu} + \int_{\mu_{min}}^{a-z} dw\, P(w)\, (1 - \frac{a-z}{w}) \right] , \qquad \text{(A-27)}$$

where

$$\frac{\bar{I}}{\mu} = \int_{\mu_{min}}^{\mu_{max}} dw\, \frac{P(w)}{w} . \qquad \text{(A-28)}$$

Let us look now at the general behavior of C(z) in three regions:

(i) $(a - z) < \mu_{min}$: the integral vanishes, since $P(w) = 0$ and Eq. (A-27) reduces to the same form as Eq. (A-3), where $\frac{1}{\mu}$ is replaced by $\frac{\bar{I}}{\mu}$;

(ii) $\mu_{min} < (a - z) < \mu_{max}$: the integral does not vanish in general and depends on what function is chosen for P(w).

(iii) $(a - z) > \mu_{max}$: this is in the internal region, and $C(z) = C_0$.

Appendix B
CALCULATION OF THE FRACTIONAL RELEASE

1. Slab

With the notation

$$\frac{\partial}{\partial x}\,(\,) \equiv (\,)_x, \qquad \frac{\partial^2}{\partial x^2}\,(\,) \equiv (\,)_{xx}, \text{ etc.},$$

the concentration $C(z,t)$ at any time t after diffusion started is a solution of the following problem:

$$C_t = D\,C_{zz}, \qquad \text{for } -a < z < a, \quad 0 < t. \tag{B-1a}$$

$$\left.\begin{aligned} C(z,0) &= C_0, && \text{for } -(a-\mu) < z < (a-\mu), \\ &= \frac{C_0}{2\mu}\,(a+\mu \pm z), && \text{for } (a-\mu) < \mp z < a, \end{aligned}\right\} \tag{B-1b}$$

$$C(\pm a, t) = 0, \qquad 0 \leqslant t \tag{B-1c}$$

where the initial condition given by Eq. (B-1b) was derived in Appendix A.

Making the substitutions

$$U = \frac{C}{C_0}, \quad x = \frac{z}{a}, \quad \epsilon = \frac{\mu}{a}, \quad \tau = \frac{Dt}{a^2} \tag{B-2}$$

gives a dimensionless form:

$$U_\tau = U_{xx}, \qquad \text{for } -1 < x < 1, \quad 0 < \tau. \tag{B-3a}$$

$$\left.\begin{aligned} U(x,0) &= 1, && \text{for } -(1-\epsilon) < x < (1-\epsilon), \\ &= \frac{1+\epsilon \pm x}{2\epsilon} && \text{for } (1-\epsilon) < \mp x < 1, \end{aligned}\right\} \tag{B-3b}$$

$$U(\pm 1, \tau) = 0, \qquad \text{for } 0 \leqslant \tau. \tag{B-3c}$$

Let $G(w, x, \tau)$ be Green's function for a slab with the same boundary conditions as given by Eq. (B-3c); a formal solution is then

given by

$$U(x, \tau) = \int_{-1}^{1} dw\ U(w, 0)\ G(w, x, \tau)\ . \tag{B-4}$$

The Laplace transform with the notation

$$\bar{V}(x, q) \equiv \int_{0}^{\infty} d\tau\ V(x, \tau)\ e^{-p\tau}, \tag{B-5}$$

where $p = q^2$ is applied to Eq. (B-4):

$$\bar{U}(x, q) = \int_{-1}^{1} dw\ \ U(w, 0)\ \bar{G}\,(w, x, q)\ . \tag{B-6}$$

The function $\bar{G}$ is given in reference C1, and is equal to

$$\bar{G}(w, x, q) = \begin{cases} g(w, x), & \text{for } w < x \\ \\ g(x, w), & \text{for } x < w, \end{cases} \tag{B-7}$$

where

$$g(w, x) = \frac{\sinh(1 + w)\ \sinh(1 - w)}{q\ \sinh 2q}\ . \tag{B-8a}$$

Notice the important property of g,

$$g(x, w) = g(-w, -x). \tag{B-8b}$$

By substituting Eqs. (B-3b) and (B-7) into Eq. (B-6), we obtain

$$\bar{U}(x, q) = \int_{-1}^{-(1-\epsilon)} dw\ S(-w)\ g(w, x) + \int_{-(1-\epsilon)}^{(1-\epsilon)} dw\ g(w, x) + \int_{1-\epsilon}^{x} dw\ S(w)\ g(w, x)$$

$$+ \int_{x}^{1} dw\ S(w)\ g(x, w) \qquad \text{for } 1 - \epsilon < x < 1, \tag{B-9}$$

where

$$S(x) = \frac{1 + \epsilon - x}{2\epsilon} \quad . \tag{B-10}$$

Differentiating and evaluating the derivative at $x = 1$, we have

$$\bar{U}_x(1, q) = \int_{-1}^{-(1-\epsilon)} dw\, S(-w)\, g_x(w, 1) + \int_{-(1-\epsilon)}^{1-\epsilon} dw\, g_x(w, 1) + \int_{1-\epsilon}^{1} dw\, S(w)\, g_x(w, 1); \tag{B-11}$$

substituting for S and g_x, we obtain

$$\bar{U}_x(1, q) = - \frac{1}{\sinh 2q} \left[\int_{-(1-\epsilon)}^{1-\epsilon} dw\, \sinh q(1+w) + \frac{1}{2\epsilon} \int_{1-\epsilon}^{1} dw(1+\epsilon-w) \Big(\sinh q(1+w) + \sinh q(1-w) \Big) \right] . \tag{B-12}$$

Upon performing the integration and some rearrangement, we obtain

$$\bar{U}_x(1, q) = - \frac{1}{2q} \frac{1}{\cosh q} \left(\sinh q + \frac{2}{\epsilon q} \sinh \frac{2-\epsilon}{2} q \sinh \frac{\epsilon}{2} q \right) . \tag{B-13}$$

Let $Q(t)$ be the number of tracer atoms at time t within a parallelepiped that cuts a unit area at each face of the slab $z = a$ and $z = -a$, in units of $2aC_0$; then, by Fick's first law we have (remember we have <u>two</u> faces)

$$Q_t = 2 \frac{D}{2aC_0} C_z(a, t), \tag{B-14}$$

where $Q_t = \frac{dQ}{dt}$; we make now the substitutions of Eqs. (B-2) and obtain

$$Q_\tau = U_x(1, \tau). \tag{B-15}$$

We apply the Laplace transform to Eq. (B-15):

$$q^2 \bar{Q}(q) - Q(0) = \bar{U}_x(1, q). \tag{B-16}$$

From Eqs. (B-13) and (B-16) we obtain

$$\bar{Q}(q) = \frac{Q_0}{q^2} - \frac{1}{2q^3}\left[\tanh q + \frac{\sinh\frac{2-\epsilon}{2}}{\cosh q} \quad \frac{\sinh\frac{\epsilon}{2}q}{\frac{\epsilon}{2}q}\right], \qquad \text{(B-17)}$$

where $Q_0 = Q(0)$; using properties of hyperbolic functions, we further simplify to

$$\bar{Q}(q) = \frac{Q_0}{q^2} - \frac{1}{2q^3}\left\{\tanh q + \frac{1}{\epsilon q}\left[1 - \frac{\cosh q(1-\epsilon)}{\cosh q}\right]\right\}. \qquad \text{(B-18)}$$

Now, using a procedure similar to that applied by Berthier in solving a problem involving uniform initial concentration,[B2] we expand the hyperbolic functions in series of exponentials:

$$\bar{Q}(q) = \frac{Q_0}{q^2} - \frac{1}{q^3}\left(\frac{1}{2} - e^{-2q} + e^{-4q} - e^{-6q} + \cdots\right)$$

$$- \frac{1}{2\epsilon q^4}\left\{1 - e^{-\epsilon q} + \left[e^{-q(2+\epsilon)} - e^{-q(2-\epsilon)}\right] - \left[e^{-q(4+\epsilon)} - \cdots\right] \cdots\right\}. \qquad \text{(B-19)}$$

Performing the inversion term by term, we obtain

$$Q_0 - Q(\tau) = \left[1 + \pi^{1/2}\frac{2\tau^{1/2}}{\epsilon}\left(\frac{1}{4} - i^2\mathrm{erfc}\frac{\epsilon}{2\tau^{1/2}}\right)\right]\frac{\tau^{1/2}}{\pi^{1/2}}$$

$$- \left[i\mathrm{erfc}\frac{1}{\tau^{1/2}} - i\mathrm{erfc}\frac{2}{\tau^{1/2}} + i\mathrm{erfc}\frac{3}{\tau^{1/2}} - \cdots\right]2\tau^{1/2}$$

$$+ \left[i^2\mathrm{erfc}\left(\frac{1}{\tau^{1/2}} + \frac{\epsilon}{2\tau^{1/2}}\right) - i^2\mathrm{erfc}\left(\frac{1}{\tau^{1/2}} - \frac{\epsilon}{2\tau^{1/2}}\right)\right.$$

$$\left. - \left\{i^2\mathrm{erfc}\left(\frac{2}{\tau^{1/2}} + \frac{\epsilon}{2\tau^{1/2}}\right) - i^2\mathrm{erfc}\left(\frac{2}{\tau^{1/2}} - \frac{\epsilon}{2\tau^{1/2}}\right)\right\} + \cdots\right]\frac{2\tau}{\epsilon}. \qquad \text{(B-20)}$$

Equation (B-20) gives us the cumulative number of tracer atoms in units of $2aC_0$ released through both faces from a parallelepiped that cuts a unit area at each face. The fractional release $f(\tau)$ is defined as

$$f(\tau) = \frac{Q_0 - Q(\tau)}{Q_0} , \tag{B-21}$$

where

$$Q_0 = \frac{1}{2aC_0} \int_{-a}^{a} dw\, C(w, 0) . \tag{B-22}$$

Substituting for $C(w, 0)$ from Eq. (B-1b) and carrying the integration through, we obtain

$$Q_0 = 1 - \frac{\epsilon}{2} , \tag{B-23}$$

hence

$$f(\tau) = \frac{1}{1-\frac{\epsilon}{2}} (Q_0 - Q(\tau)), \tag{B-24}$$

and, in the special case $\epsilon >> 1$,

$$f(\tau) \approx Q_0 - Q(\tau), \qquad \text{for } \epsilon << 1. \tag{B-25}$$

Assuming the approximation of Eq. (B-25) to be valid, we verify now that $f(\tau)$ as given by Eqs. (B-25) and (B-20) is properly connected to the well-known solution with no recoil in the two asymptotic cases $\theta \to \infty$ and $\theta \to 0$, where $\theta = \epsilon/2\tau^{1/2}$.

a. The case $\theta \to \infty$

This represents a physical situation in which diffusion has just started, i.e., $\tau \to 0$. Since concentration on the surface is just $C_0/2$, we expect in this limiting case to have a release equal to half of that with no recoil where concentration on the surface is C_0. We use the property

$$i^2\text{erfc}\frac{1}{v} \approx \frac{v}{2}\ \text{ierfc}\frac{1}{v}, \quad \text{for } v \ll 1, \tag{B-26}$$

(see Appendix D) to show that for small $\tau^{1/2}$ the third term in Eq. (B-20) may be approximated by the expression

$$\left[\left(\frac{1}{1+\frac{\epsilon}{2}}\ \text{ierfc}\ \frac{1+\frac{\epsilon}{2}}{\tau^{1/2}} - \frac{1}{1-\frac{\epsilon}{2}}\ \text{ierfc}\ \frac{1-\frac{\epsilon}{2}}{\tau^{1/2}}\right)\right.$$

$$\left. - \left(\frac{1}{2+\frac{\epsilon}{2}}\ \text{ierfc}\ \frac{2+\frac{\epsilon}{2}}{\tau^{1/2}} - \frac{1}{2-\frac{\epsilon}{2}}\ \text{ierfc}\ \frac{2-\frac{\epsilon}{2}}{\tau^{1/2}}\right) + \left(\ldots\right)\right]\frac{\tau}{\epsilon}$$

and hence may be neglected in comparison with terms of order of $\tau^{1/2}$, so that in the case of small $\tau^{1/2}$ Eq. (B-20) goes over to

$$f(\tau) \approx \frac{\tau^{1/2}}{\pi^{1/2}} - 2\left(\text{ierfc}\frac{1}{\tau^{1/2}} - \text{ierfc}\frac{2}{\tau^{1/2}} + \text{ierfc}\frac{3}{\tau^{1/2}} - \cdots\right)\tau^{1/2}, \tag{B-27}$$

which gives half of the fractional release with no recoil as was expected (compare Eq. (4) in Sec. 12.5 of reference C1).

b. <u>The case $\theta \to 0$</u>

This case represents a physical situation in which the recoil range is so small that the initial concentration practically approaches a uniform distribution. Therefore at the limit $\theta = 0$ we expect a release identical to that given by the nonrecoil case. Using asymptotic expansion of $i^2\text{erfc}\theta$ for small θ, we have

$$\lim_{\theta\to 0}\ \frac{\pi^{1/2}}{\theta}\left(\frac{1}{4} - i^2\text{erfc}\theta\right) = \lim_{\theta\to 0}\ \frac{\pi^{1/2}}{\theta}\left(\frac{1}{4} - \frac{1}{4} + \frac{\theta}{\pi^{1/2}} - o(\theta^2)\right) = 1; \tag{B-28}$$

also, note that by the usual definition of a derivative we have

$$\lim_{\theta\to 0}\ \frac{1}{\theta}\left[i^2\text{erfc}\left(\frac{1}{\tau^{1/2}}+\theta\right) - i^2\text{erfc}\left(\frac{1}{\tau^{1/2}}-\theta\right)\right] = 2\,\frac{d}{d\,\frac{1}{\tau^{1/2}}}\ i^2\text{erfc}\ \frac{1}{\tau^{1/2}}, \tag{B-29}$$

and by definition of i^nerfcv we obtain

$$2 \frac{d}{d \frac{1}{\tau^{1/2}}} i^2\text{erfc } \frac{1}{\tau^{1/2}} = -2 \text{ ierfc } \frac{1}{\tau^{1/2}}, \qquad \text{(B-30)}$$

and similarly for the rest of the terms in the third brackets of Eq. (B-20). So from Eqs. (B-20), (B-28), (B-29), and (B-30), we obtain

$$\lim_{\theta \to 0} f(\tau) \approx \frac{2}{\pi^{1/2}} \tau^{1/2} - 4\tau^{1/2}\left(\text{ierfc } \frac{1}{\tau^{1/2}} - \text{ierfc } \frac{2}{\tau^{1/2}} + \cdots\right), \qquad \text{(B-31)}$$

which is identical to the fractional release with no recoil, as was expected. (compare Eq. (4) in Sec. 12.5 of reference C1).

2. Infinite Cylinder

We shall approximate the initial concentration with one of a solid that has a flat surface, which was derived in Appendix A; the problem statement is

$$C_t = D\,(C_{rr} + \frac{1}{r} C_r), \qquad \text{for } 0 \leq r < a, \qquad 0 < t \qquad \text{(B-32a)}$$

$$\left.\begin{aligned} C(r, 0) &= C_0 && \text{for } 0 \leq r < (a - \mu), \\ &= \frac{C_0}{2\mu}(a + \mu - r) && \text{for } (a-\mu) \leq r < a, \end{aligned}\right\} \qquad \text{(B-32b)}$$

$$C(a, t) = 0, \qquad \text{for } 0 \leq t, \qquad \text{(B-32c)}$$

When we use the substitutions of Eq. (B-2) with z replaced by r, the problem goes over to

$$U_\tau = U_{xx} + \frac{1}{x} U_x, \qquad \text{for } 0 \leq x < 1, \qquad 0 < \tau, \qquad \text{(B-33a)}$$

$$\left.\begin{aligned} U(x, 0) &= 1 && \text{for } 0 \leq x < 1 - \epsilon, \\ &= \frac{1}{2\epsilon}(1 + \epsilon - x), && \text{for } 1 - \epsilon < x < 1, \end{aligned}\right\} \qquad \text{(B-33b)}$$

$$U(1, \tau) = 0, \qquad \text{for } 0 \leq \tau. \qquad \text{(B-33c)}$$

The solution method follows essentially the same procedure as used in solving the slab problem in Section B. 1. We write a formal solution using Green's function,

$$U(x, \tau) = 2\pi \int_0^1 dw\, w\, U(w, 0)\, G(w, x, \tau), \tag{B-34}$$

then we apply Laplace transformation as defined by Eq. (B-5),

$$\bar{U}(x, q) = 2\pi \int_0^1 dw\, w\, U(w, 0)\, \bar{G}(w, x, q), \tag{B-35}$$

where $\bar{G}$ is given in reference C1,

$$2\pi\, \bar{G}(w, x, q) = \begin{cases} g(w, x) & \text{for } w < x \\ g(x, w) & \text{for } x < w, \end{cases} \tag{B-36}$$

where

$$g(w, x) = \frac{I_0(q, w)}{I_0(q)} \left[I_0(q)\, K_0(qx) - I_0(qx\, K_0(q) \right] \tag{B-37}$$

and from Eqs. (B-33b), (B-35), and (B-36) we have

$$\bar{U}(x, q) = \int_0^{1-\epsilon} dw\, w\, g(w, x) + \frac{1}{2\epsilon} \int_{1-\epsilon}^{x} dw\, w\, (1 + \epsilon - w)\, g(w, x)$$

$$+ \frac{1}{2\epsilon} \int_x^1 dw\, w\, (1 + \epsilon - w)\, g(x, w), \quad \text{for } 1 - \epsilon < x < 1. \tag{B-38}$$

We now differentiate both sides of Eq. (B-38) with respect to x and evaluate at x = 1, making use of g(1, 1) = 0. We obtain

$$\bar{U}_x(1, q) = \int_0^{1-\epsilon} dw\, w\, g_x(w, 1) + \frac{1+\epsilon}{2\epsilon} \int_{1-\epsilon}^{1} dw\, w\, g_x(w, 1) - \frac{1}{2\epsilon} \int_{1-\epsilon}^{1} dw\, w^2\, g_x(w, 1).$$

(B-39)

From Eq. (B-37) we have

$$g_x(w, 1) = - \frac{I_0(wq)}{I_0(q)} . \qquad \text{(B-40)}$$

Substituting this into Eq. (B-39) and evaluating the integrals, we obtain

$$\bar{U}_x(1, q) = - \frac{1}{2q} \frac{I_1(q)}{I_0(q)} - \frac{1}{2\epsilon q^3} \int_{(1-\epsilon)q}^{q} dw\, w \frac{I_1(w)}{I_0(q)} . \qquad \text{(B-41)}$$

Now, if Q(t) is the number of tracer atoms in units of $\pi a^2 C_0$ per unit height of the cylinder at time t, then by Fick's first law we have

$$Q_t = \frac{2\pi a}{\pi a^2 C_0} D C_r, \qquad \text{(B-42)}$$

or, in the dimensionless form [make the substitutions of Eq. (B-2)], we have

$$Q_\tau = 2 U_x(1, q). \qquad \text{(B-43)}$$

We also have, in gereral,

$$q^2 \bar{Q} - Q_0 = \bar{Q}_\tau , \qquad \text{(B-44)}$$

so, combining Eqs. (B-41), (B-43), and (B-44), we obtain

$$\bar{Q}(q) = \frac{Q_0}{q^2} - \frac{1}{q^3} \frac{I_1(q)}{I_0(q)} - \frac{1}{\epsilon q^5} \int_{(1-\epsilon)q}^{q} dw\, w \frac{I_1(w)}{I_0(q)} . \qquad \text{(B-45)}$$

We expand now the second and third terms, using the semi-convergent series[H2]

$$I_1(q) = \frac{e^q}{(2\pi q)^{1/2}} \left(1 - \frac{3}{8q} - \frac{15}{2(8q)^2} - \frac{105}{2(8q)^3} - \cdots\right), \tag{B-46}$$

$$I_0(q) = \frac{e^q}{(2\pi q)^{1/2}} \left(1 + \frac{1}{8q} + \frac{9}{2(8q)^2} + \frac{75}{2(8q)^3} - \cdots\right), \tag{B-47}$$

from which we obtain

$$\frac{I_1(q)}{I_0(q)} = 1 - \frac{1}{2q} - \frac{1}{8q^2} - \frac{1}{8q^3} - \cdots ; \tag{B-48}$$

also, in calculating the third term in Eq. (B-45) we have

$$\frac{1}{I_0(q)} \int_{(1-\epsilon)q}^{q} dw\, w\, I_1(w)$$

$$= q^{1/2} e^{-q} \left(1 - \frac{1}{8q} - \frac{7}{2(8q)^2} - \frac{59}{2(8q)^3} \cdots\right) \int_{(1-\epsilon)q}^{q} dw\, w^{1/2} e^{w} \left(1 - \frac{3}{8w} - \frac{15}{2(8w)^2} - \frac{105}{2(8w)^3} \cdots\right)$$

$$= q^{1/2} e^{-q} \left(1 - \frac{1}{8q} - \frac{7}{2(8q)^2} - \frac{59}{2(8q)^3} \cdots\right) \left[e^{w} w^{1/2} \left(1 - \frac{7}{8w} - \frac{71}{2(8w)^2} - \frac{957}{2(8w)^3} \cdots\right) \right]_{(1-\epsilon)q}^{q}$$

$$= \left[1 - (1-\epsilon)^{1/2} e^{-\epsilon q}\right] q - \left[1 - \frac{1 - \frac{\epsilon}{8}}{(1-\epsilon)^{1/2}} e^{-\epsilon q}\right] - \left[1 - \frac{1 + \frac{7\epsilon^2}{64}}{(1-\epsilon)^{3/2}} e^{-\epsilon q}\right] \frac{1}{2q}$$

$$- \left[1 - \frac{1 - \frac{\epsilon}{112} + \frac{\epsilon^2}{7} - \frac{59\epsilon^3}{896}}{(1-\epsilon)^{5/2}} e^{-\epsilon q}\right] \frac{7}{8q^2} , \tag{B-49}$$

where terms of the order of ϵ^4 and smaller terms were neglected.

Inverting Eqs. (B-48) and (B-49) term by term, we obtain

$$L^{-1}\left[\frac{1}{q^3}\,\frac{I_1(q)}{I_0(q)}\right] = \frac{2}{\pi^{1/2}}\,\tau^{1/2} - \frac{1}{2}\,\tau - \frac{1}{6\pi^{1/2}}\,\tau^{3/2} - \frac{1}{16}\,\tau^2 - \cdots, \tag{B-50}$$

$$L^{-1}\left[\frac{1}{\epsilon q^5}\int_{(1-\epsilon)}^{q} dw\, w\,\frac{I_1(w)}{I_0(q)}\right] = \frac{1}{2\theta}\left[(1 - 4(1-\epsilon)^{1/2} i^2\mathrm{erfc}\,\theta)\tau^{1/2}\right.$$

$$\left. -\left(\frac{1}{6\pi^{1/2}} - \frac{1-\frac{\epsilon}{8}}{(1-\epsilon)^{1/2}}\, i^3\mathrm{erfc}\,\theta\right)8\tau - \left(\frac{1}{32} - \frac{1+\frac{7\epsilon^2}{64}}{(1-\epsilon)^{3/2}}\, i^4\mathrm{erfc}\,\theta\right)8\tau^{3/2} - \cdots\right], \tag{B-51}$$

where $\theta = \frac{\epsilon}{2\tau^{1/2}}$. From Eqs. (B-45), (B-50), and (B-51) we have

$$Q_0 - Q(\tau) = \frac{2}{\pi^{1/2}}(1+\alpha)\,\tau^{1/2} - \frac{1}{2}(1+\beta)\,\tau - \frac{1}{6\pi^{1/2}}(1+\gamma)\,\tau^{3/2} \cdots \tag{B-52}$$

where α, β, and γ depend on τ and are given by

$$\alpha = \frac{\pi^{1/2}}{\theta}\left(\frac{1}{4} - (1 - 2\tau^{1/2}\theta)^{1/2} i^2\mathrm{erfc}\,\theta\right),$$

$$\beta = \frac{8}{\theta}\left(\frac{1}{6\pi^{1/2}} - \frac{1 - \frac{\tau^{1/2}\theta}{4}}{(1 - 2\tau^{1/2}\theta)^{1/2}}\, i^3\mathrm{erfc}\,\theta\right), \tag{B-53}$$

$$\gamma = \frac{24\pi^{1/2}}{\theta}\left(\frac{1}{32} - \frac{1 + \frac{7\tau\theta^2}{46}}{(1 - 2\tau^{1/2}\theta)^{1/2}}\, i^4\mathrm{erfc}\,\theta\right).$$

In this case

$$Q_0 = \frac{1}{\pi a^2 C_0}\int_0^a dw\, 2\pi\, w\, C(w, 0). \tag{B-54}$$

Substituting for C(w, 0) from Eq. (B-32b) and carrying through the integration, we obtain

$$Q_0 = 1 - \frac{\epsilon}{2} + \frac{\epsilon^2}{6} \quad . \tag{B-55}$$

Hence, from the definition of $f(\tau)$ [Eq. (B-21)],

$$f(\tau) = \frac{1}{1 - \frac{\epsilon}{2} + \frac{\epsilon^2}{6}} \, (Q_0 - Q(\tau)), \tag{B-56}$$

and in the special case for $\epsilon \ll 1$,

$$f(\tau) \approx Q_0 - Q(\tau), \quad \text{for } \epsilon \ll 1. \tag{B-57}$$

If this Eq. (B-57) is a good solution we expect the two asymptotic cases $\theta \to \infty$ and $\theta \to 0$ to properly go over to the solution with no recoil.

a. The case $\theta \to \infty$

Release "has just started," hence we expect the release to be just half of that with a uniform initial concentration.

Since we have

$$\lim_{\theta \to \infty} i^n \text{erfc}\theta = 0 \quad \text{for } n = 0, 1, 2, \cdots, \tag{B-58}$$

it is easy to see that

$$\lim_{\theta \to \infty} \alpha = 0, \qquad \lim_{\theta \to \infty} \beta = 0, \qquad \lim_{\theta \to \infty} \gamma = 0, \tag{B-59}$$

and therefore

$$\lim_{\theta \to \infty} f(\tau) = \frac{2}{\pi^{1/2}} \tau^{1/2} - \frac{1}{2}\tau - \frac{1}{6\pi^{1/2}} \tau^{3/2}, \tag{B-60}$$

which is just half of the well-known fractional release without recoil, [C3] as expected.

b. The case $\theta \to 0$

The effect of recoil must diminish and the release should be identical to that in the case of uniform initial concentration.

Calculating α, β, and γ by using asymptotic expansions for small θ (see Appendix D), we obtain

$$\lim_{\theta \to 0} \alpha = \lim_{\theta \to 0} \frac{\pi^{1/2}}{\theta} \left[\frac{1}{4} - (1 - \tau^{1/2}\theta - \cdots)\left(\frac{1}{4} - \frac{\theta}{\pi^{1/2}} + \cdots\right) \right] = 1 + \frac{\pi^{1/2}}{4} \tau^{1/2},$$

$$\lim_{\theta \to 0} \beta = \lim_{\theta \to 0} \frac{8}{\theta} \left[\frac{1}{6\pi^{1/2}} - (1 + \frac{3}{4} \tau^{1/2}\theta - \cdots)\left(\frac{1}{6\pi^{1/2}} - \frac{\theta}{4} + \cdots\right) \right] = 2 - \frac{\tau^{1/2}}{\pi^{1/2}},$$

$$\lim_{\theta \to 0} \gamma = \lim_{\theta \to 0} \left[\frac{24\pi^{1/2}}{\theta} \frac{1}{32} - (1 + 3\tau^{1/2}\theta - \cdots)\left(\frac{1}{32} - \frac{\theta}{6\pi^{1/2}} + \cdots\right) \right] = 4 - \frac{9}{4}\pi^{1/2}\tau^{1/2}.$$

(B-61)

Substituting Eq. (B-61) into Eqs. (B-52) and (B-57), we obtain

$$\lim_{\theta \to 0} f(\tau) = \frac{4}{\pi^{1/2}} \tau^{1/2} - \tau - \frac{1}{3\pi^{1/2}} \tau^{3/2} \cdots, \qquad \text{(B-62)}$$

which is identical to the fractional release without recoil, as expected.

3. Finite Cylinder

In constructing a solution to the finite cylinder with a radius a and half height h, we now utilize the solutions for a slab and an infinite cylinder derived in Sections B. 1 and B. 2. We assume that $\frac{\mu}{a}$ and $\frac{\mu}{h}$ are small compared with unity; this assumption is necessary in order to make the following two major approximations.

a. Approximate the recoil-depleted distribution near the curved surface of the cylinder by one near a flat surface. It was shown in Appendix A that this introduces an error in the concentration that is bounded by $\frac{\mu}{2a}$.

b. Assume that the initial distribution in the region near the edge of the cylinder $(a-\mu) < r < a$, $(h-\mu) < |z| < h$, is equal to the product of the initial distributions in r and z. Analysis similar to the one done in Appendix A shows that this gives the correct value $\frac{C}{C_0} = \frac{1}{4}$ right on the edge, but an incorrect value anywhere else. It turns out, however, that contribution from the region near the edge to the release from the whole cylinder is relatively small. It is easy to see that the ratio of release from the region near the edge of the cylinder to release from the whole cylinder is of the order of

$$\frac{(2\pi a\,\mu)\,4}{2\pi a^2 + 4\pi a h} = \frac{4\mu}{a + 2h} .$$

Hence the error introduced by this assumption is clearly bounded by this ratio, and can be neglected for $\frac{\mu}{a} \ll 1$ and $\frac{\mu}{h} \ll 1$.

The problem for the finite cylinder with radius a and height 2h can be now stated as

$$C_t = D(C_{rr} + \frac{1}{r} C_r + C_{zz}), \quad \text{for } 0 < r < a, \quad 0 < |z| < h, \quad 0 < t, \qquad \text{(B-63)}$$

$$
\left.
\begin{aligned}
C(r, z, 0) &= C_0 && \text{for } 0 < r < (a-\mu),\ 0 < |z| < (h-\mu), \\
&= \frac{C_0}{2\mu}\,(a+\mu-r) && \text{for } (a-\mu) < r < a,\ 0 < |z| < (h-\mu), \\
&= \frac{C_0}{2\mu}\,(h+\mu-z) && \text{for } 0 < r < (a-\mu),\ (h-\mu) < |z| < h, \\
&= \frac{C_0}{4\mu^2}\,(a+\mu-r)(h+\mu-z), && (a-\mu) < r < a,\ (h-\mu) < |z| < h,
\end{aligned}
\right\} \quad \text{(B-64)}
$$

$$
C(a, z, t) = C(r, \pm h, t) = 0, \qquad \text{for } 0 \leq t. \qquad \text{(B-65)}
$$

We construct a solution form

$$
\psi(r, z, t) = A\,\rho(r, t)\,Z(z, t), \qquad \text{(B-66)}
$$

where A is a constant to be adjusted to meet the initial conditions,

ρ is the solution of an infinite cylinder of radius a with recoil,

Z is the solution of a slab of thickness 2h with recoil.

The function ψ has the following properties

(a) It satisfies the differential equation (B-63).

(b) It satisfies the initial condition, Eq. (B-64).

(c) It satisfies the boundary condition, Eq. (B-65).

By the uniqueness theorem[C1] it is therefore the only solution.

The functions ρ and Z are in general of the form

$$
x = \sum_{n=1}^{\infty} A_n\,x_n\,\exp(-\lambda_n t)\,, \qquad \text{(B-67)}
$$

where x_n and λ_n are the space eigenfunctions and eigenvalues respectively. This kind of function converges very slowly for small times, and hence is very difficult to evaluate.[J1] For this reason we use the solutions valid for small times that were developed in Sections 1 and 2, and which are easy to evaluate.

Let $Z(z,t)$ and $\rho(r,t)$ be these solutions for small times for a slab and an infinite cylinder respectively, then

$$C(r,z,t) = B\, Z(z,t)\, \rho(r,t), \tag{B-68}$$

valid for small times. The fraction of tracer atoms yet not released is given by

$$1 - f(\tau) = \frac{\int_0^a dr\, r\, \rho(r,t)}{\int_0^a dr\, r\, \rho(r,0)} \; \frac{\int_0^h dz\, Z(z,t)}{\int_0^h dz\, Z(z,0)}, \tag{B-69}$$

where $f(\tau)$ is the fractional release that is the cumulative number of tracer atoms released from the cylinder at time t (or τ) divided by the number of tracer atoms that were contained in the cylinder at time t = 0. The first ratio in Eq. (B-69) is equal to $\frac{Q(\tau)}{Q_0}$ for an infinite cylinder, the second ratio is equal to $\frac{Q(\tau)}{Q_0}$ for a slab. Let us denote Q by Q^a for an infinite cylinder and Q^h for a slab, then, from Eq. (B-69) we have

$$f(\tau) = 1 - \frac{Q^a(\tau)}{Q_0^a} \; \frac{Q^h(\tau)}{Q_0^h}$$

$$= 1 - \left(1 - \frac{Q_0^a - Q^a(\tau)}{Q_0^a}\right)\left(1 - \frac{Q_0^h - Q^h(\tau)}{Q_0^h}\right). \tag{B-70}$$

Combining this with Eq. (B-21), we obtain

$$f(\tau) = 1 - [1 - f^a(\tau)]\,[1 - f^h(\tau)]$$

$$= f^a(\tau) + f^h(\tau) - f^a(\tau)\, f^h(\tau), \tag{B-71}$$

where f^h and f^a are the fractional release from a slab and infinite cylinder and are given by Eqs. (B-20) and (B-25) and by (B-52) and (B-57), respectively.

4. Finite Cylinder: Reduction to a Simple Form

The dependence of the cumulative release, f, on time is given by Eq. (B-71), which in general is not easy to evaluate. We now take advantage of the following three conditions, which will be satisfied by the planned experiment,

$$\tau < 10^{-4}, \qquad \text{(B-72a)}$$

$$0 < \mu < 12 \text{ microns}, \qquad \text{(B-72b)}$$

$$a = h = 2500 \text{ microns}, \qquad \text{(B-72c)}$$

and reduce Eq. (B-71) to a simpler form which we shall use throughout the analysis. The first condition is assumed on the basis of data from a postirradiation anneal experiment[L4] extrapolated to higher temperatures. The second assumed condition is nothing more than a guess based on the experimental finding[E1] that the fission recoil range in urania of fragments of the heavy group was roughly 6 microns.

Under the above conditions we can make the following approximations:

$$\tau^{1/2} \pm \tau^{n/2} \approx \tau^{1/2}, \qquad \text{for } n = 2, 3, 4, \qquad \text{(B-73a)}$$

$$1 \pm i^n \text{erfc} \frac{m}{\tau^{1/2}} \approx 1, \qquad \text{for } n = 0, 1, 2, \; m \geq 1/2, \qquad \text{(B-73b)}$$

$$1 \pm \epsilon^n \approx 1, \qquad \text{for } n = 1, 2, 3. \qquad \text{(B-73c)}$$

With these approximations, Eq. (B-71) reduces to

$$f(\tau) \approx (1 + \Phi(\tau)) \frac{\tau^{1/2}}{\pi^{1/2}} + 2(1 + \Phi(\tau)) \frac{\tau^{1/2}}{\pi^{1/2}} + o(\tau)$$

$$\approx \frac{3}{\pi^{1/2}} (1 + \Phi(\tau)) \tau^{1/2}, \qquad \text{(B-74)}$$

where

$$\Phi = \frac{\pi^{1/2}}{\theta} \left(\frac{1}{4} - i^2\text{erfc}\theta\right), \quad \theta = \frac{\epsilon}{2\tau^{1/2}}, \quad \epsilon = \frac{\mu}{a}. \qquad \text{(B-75)}$$

The fractional release $f(\tau)$ was calculated by using tables of the functions $i^n\text{erfcv}$,[K1] and plotted in Figs. 26 and 27.

Inthoff and Zimen[I1] used an alternative method to estimate the effect of recoil. In this method a correction factor Λ_4 is calculated by which the experimental release ("recoil release") has to be multiplied in order to obtain the "nonrecoil" release. The nonrecoil release is

$$f(\text{nonrecoil}) \approx \frac{6}{\pi^{1/2}} \tau^{1/2} \qquad \text{(B-76)}$$

[see reference J1, Eq. (30)]. Hence, the correction factor mentioned above as calculated from the results of this work [i.e., Eq. (B-74)] is

$$\Lambda_1 = \frac{6}{\pi^{1/2}} \tau^{1/2} \Big/ \frac{3}{\pi^{1/2}} (1 + \Phi) \tau^{1/2}$$

$$= \frac{2}{1 + \Phi(\tau)} \cdot \qquad \text{(B-77)}$$

A discussion of Inthoff and Zimen's method and comparison with its results is presented in Appendix E.

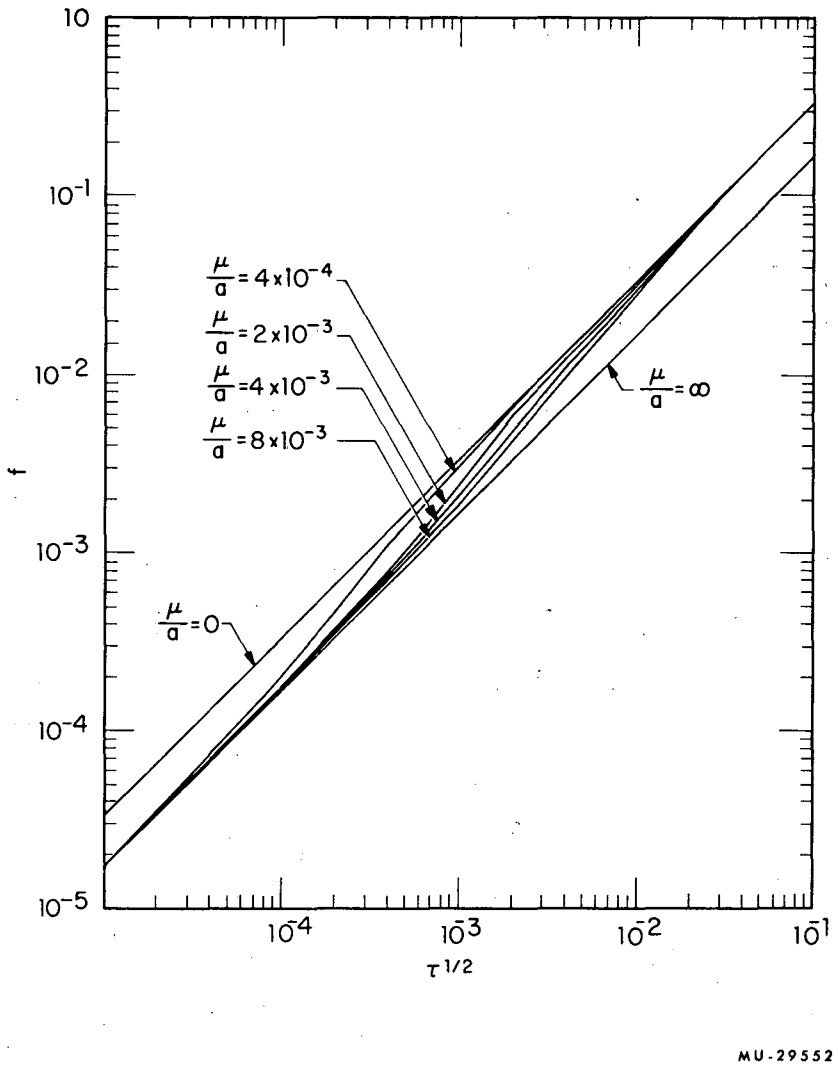

Fig. 26. Theoretical fractional release vs $\tau^{1/2}$. Cylinder height/diameter = 1. μ = recoil range; a = radius of cylinder.

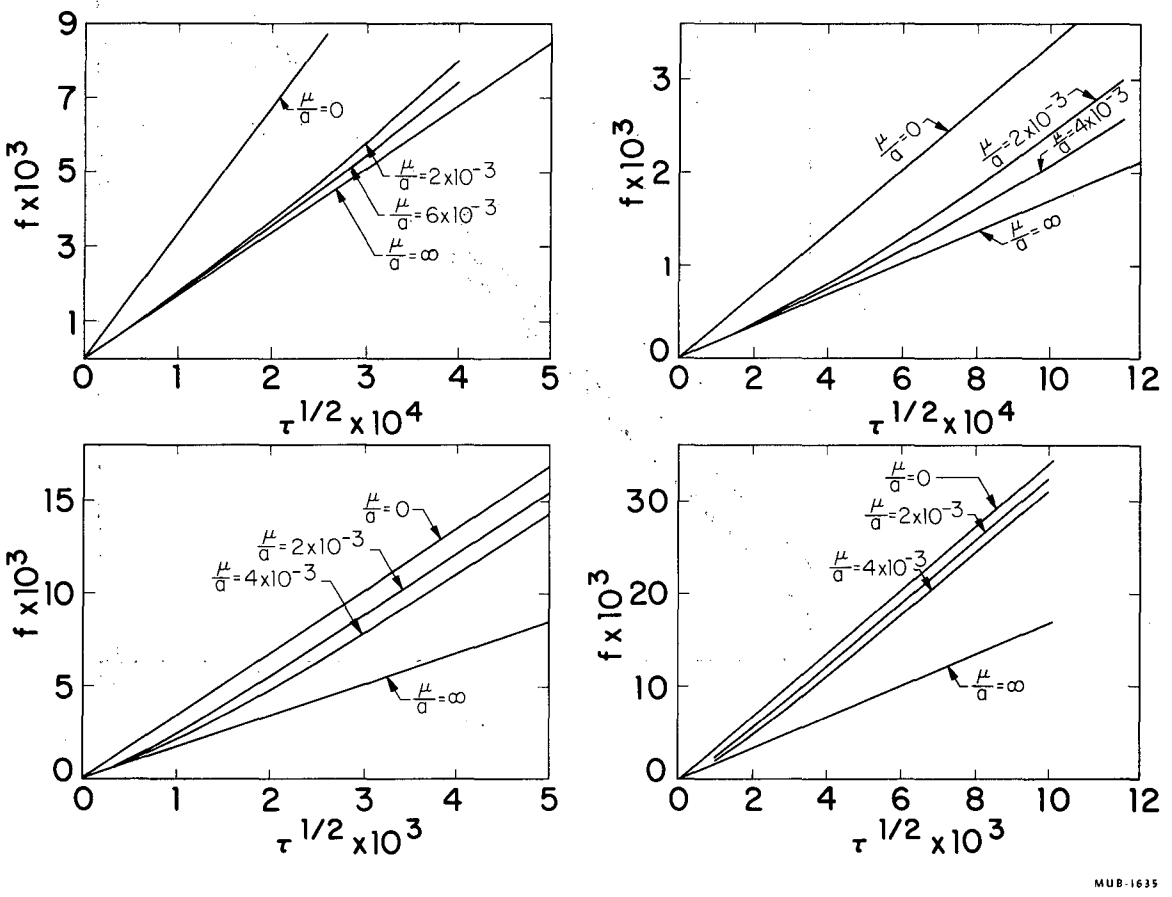

Fig. 27. Theoretical fractional release vs $\tau^{1/2}$. Cylinder height/diameter = 1. μ = recoil range; a = radius of cylinder.

Appendix C

DERIVATION OF THE RECOIL CORRECTION FUNCTION $M(\theta)$ FOR THE DIFFUSION COEFFICIENT

We start by expanding Eq. (B-74)

$$f = \frac{3}{\pi^{1/2}}\,\tau^{1/2} + \frac{3}{2}\,\frac{\tau}{\epsilon} - \frac{6}{\epsilon}\,\tau\, i^2\mathrm{erfc}\,\frac{\epsilon}{2\tau^{1/2}}\,, \tag{C-1}$$

and differentiating with respect to τ

$$\frac{df}{d\tau} = \frac{3}{2\pi^{1/2}\tau^{1/2}} + \frac{3}{2\epsilon} - \frac{6}{\epsilon}\, i^2\mathrm{erfc}\,\frac{\epsilon}{2\tau^{1/2}} - \frac{3}{2\tau^{1/2}}\,\mathrm{ierfc}\,\frac{\epsilon}{2\tau^{1/2}}\,. \tag{C-2}$$

when we rearrange, and use Eq. (D-5) of Appendix D, Eq. (C-2) reduces to

$$\frac{df}{d\tau} = \frac{3}{2\pi^{1/2}\tau^{1/2}}\left(1 + \frac{\pi^{1/2}}{2}\,\frac{\mathrm{erf}\theta}{\theta}\right) \tag{C-3}$$

or

$$\frac{df}{d\sqrt{t}} \equiv \frac{d\tau}{d\sqrt{t}}\,\frac{df}{d\tau} = \frac{3}{\pi^{1/2}}\left(\frac{D}{a^2}\right)^{1/2}\left\{1 + \frac{\pi^{1/2}}{2}\,\frac{\mathrm{erf}\theta}{\theta}\right\}, \tag{C-4}$$

from which we obtain

$$D = M(\theta)\, D_{nr}, \tag{C-5}$$

where

$$M(\theta) = \left[\frac{2}{1 + \frac{\pi^{1/2}}{2}\,\frac{\mathrm{erf}\theta}{\theta}}\right]^2, \tag{C-6}$$

and

$$D_{nr} = D(\text{nonrecoil model}) = \left[\frac{\pi^{1/2}}{6}\, a\,\frac{df}{dt^{1/2}}\right]^2. \tag{C-7}$$

With

$$a = 0.25 \text{ cm}$$

and

$$\mu = 0.0005 \text{ cm}$$

we have

$$D_{nr} = \frac{1}{183.5} \left(\frac{df}{dt^{1/2}} \right)^2 \qquad \text{(C-8)}$$

and

$$\theta = \frac{2.5 \times 10^{-4}}{(Dt)^{1/2}} \; . \qquad \text{(C-9)}$$

The function $M(\theta)$ is plotted in Fig. 11.

Appendix D

PROPERTIES OF THE INTEGRALS OF THE COMPLEMENTARY ERROR FUNCTION

We make the following definitions:[C1]

$$\text{erfcv} = \frac{2}{\pi^{1/2}} \int_v^\infty dw\, e^{-w^2}, \tag{D-1}$$

$$\text{ierfcv} = \int_v^\infty dw\, \text{erfcw}, \tag{D-2}$$

$$i^2\text{erfcv} = \int_v^\infty dw\, \text{ierfcw}, \tag{D-3}$$

$$\vdots$$

$$i^n\text{erfcv} = \int_v^\infty dw\, i^{n-1}\text{erfcw}, \tag{D-4}$$

From the above definitions we obtain the recurrence relation

$$i^n\text{erfcv} = \frac{1}{2n}\left(i^{n-2}\text{erfcv} - 2v\, i^{n-1}\text{erfcv}\right), \tag{D-5}$$

with the natural generalizations $i^0 = 1$, $i^1 = i$.

Given an asymptotic expansion for erfcv valid for small or large v,[C1] we can now, using Eq. (D-5), obtain similar asymptotic expansions for the integrals i^nerfcv.

i. Expansions valid for small v

These are convergent series:

$$\text{erfcv} = 1 - \frac{2}{\pi^{1/2}}\left(v - \frac{v^3}{1!3} + \frac{v^5}{2!5} - \frac{v^7}{3!7} \cdots\right), \tag{D-6}$$

$$\text{ierfcv} = \frac{1}{\pi^{1/2}} - v + \frac{1}{\pi^{1/2}}\left(v^2 - \frac{v^4}{6} + \frac{v^6}{30} - \frac{v^8}{168} \cdots\right), \tag{D-7}$$

$$i^2\text{erfcv} = \frac{1}{4} - \frac{v}{\pi^{1/2}} + \frac{v^2}{2} - \frac{1}{\pi^{1/2}}\left(\frac{v^3}{3} - \frac{v^5}{30} + \frac{v^7}{210} \cdots\right), \tag{D-8}$$

$$i^3\text{erfcv} = \frac{1}{6\pi^{1/2}} - \frac{v}{4} + \frac{v^2}{2\pi^{1/2}} - \frac{v^3}{6} + \frac{1}{\pi^{1/2}}\left(\frac{v^4}{12} - \frac{v^6}{180} + \frac{v^8}{1680} \cdots\right), \tag{D-9}$$

$$i^4\text{erfcv} = \frac{1}{32} - \frac{v}{6\pi^{1/2}} + \frac{v^2}{8} - \frac{v^3}{6\pi^{1/2}} + \frac{v^4}{24} - \frac{1}{\pi^{1/2}}\left(\frac{2v^5}{15} - \frac{2v^7}{305} \cdots\right), \tag{D-10}$$

ii. Expansion valid for large v

The following series are sometimes called "semiconvergent series".[H2] They do not in general converge, but they have the property that the error introduced owing to the use of only N first terms is bounded by the absolute value of the (N+1)th term:[C1]

$$\text{erfcv} = \frac{e^{-v^2}}{v\pi^{1/2}}\left(1 - \frac{1}{2v^2} + \frac{3}{4v^4} - \frac{15}{8v^6} + \frac{105}{16v^8} - \frac{945}{32v^{10}} + \cdots\right), \tag{D-11}$$

$$\text{ierfcv} = \frac{e^{-v^2}}{2v^2\pi^{1/2}}\left(1 - \frac{3}{2v^2} + \frac{15}{4v^4} - \frac{105}{8v^6} + \frac{945}{16v^8} - \frac{10395}{32v^{10}} + \cdots\right), \tag{D-12}$$

$$i^2\text{erfcv} = \frac{e^{-v^2}}{4v^3\pi^{1/2}}\left(1 - \frac{3}{v^2} + \frac{45}{4v^4} - \frac{105}{2v^6} + \frac{4725}{16v^8} - \cdots\right), \tag{D-13}$$

$$i^3\text{erfcv} = \frac{e^{-v^2}}{8v^4\pi^{1/2}}\left(1 - \frac{5}{v^2} + \frac{105}{4v^4} - \frac{315}{2v^6} + \cdots\right), \tag{D-14}$$

$$i^4\text{erfcv} = \frac{e^{-v^2}}{16v^5\pi^{1/2}}\left(1 - \frac{15}{2v^2} + \frac{105}{2v^4} - \cdots\right). \tag{D-15}$$

Appendix E
COMMENTS ON THE RECOIL CORRECTION DERIVED BY INTHOFF AND ZIMEN

The method used by Inthoff and Zimen[11] to compute the fractional release from a specimen in which the initial concentration is depleted because of fission recoil is given. This is followed by a discussion about some numerical results relevant to this method.

Method

The method is based on the two following assumptions:

(a) Fick's first law is valid.

(b) The concentration profile at any time after diffusion has started can be approximated by a straight line.

The number of tracer atoms released per unit area of a flat surface is equal to the area m(t) of the triangle shown in Fig. 28.

The area is equal to

$$m(t) = \frac{\mu}{4} C_0 \frac{\delta(t)}{2\mu - \delta(t)} \qquad \text{for } \delta \leq \mu, \qquad \text{(E-1a)}$$

$$m(t) = \frac{C_0}{2} \left(\delta(t) - \frac{\mu}{2}\right) \qquad \text{for } \delta \geq \mu. \qquad \text{(E-1b)}$$

Using assumptions (a) and (b) and Eqs. (E-1a) and (E-1b), one sets up two simple integral equations:

$$\int_0^t \frac{D}{\delta}\, dt = \frac{\mu}{4} \frac{\delta}{2\mu - \delta}, \qquad \text{for } \delta \leq \mu, \qquad \text{(E-2a)}$$

$$\int_0^t \frac{D}{\delta}\, dt = \frac{1}{2} \left(\delta - \frac{\mu}{2}\right), \qquad \text{for } \delta \geq \mu, \qquad \text{(E-2b)}$$

and solutions are

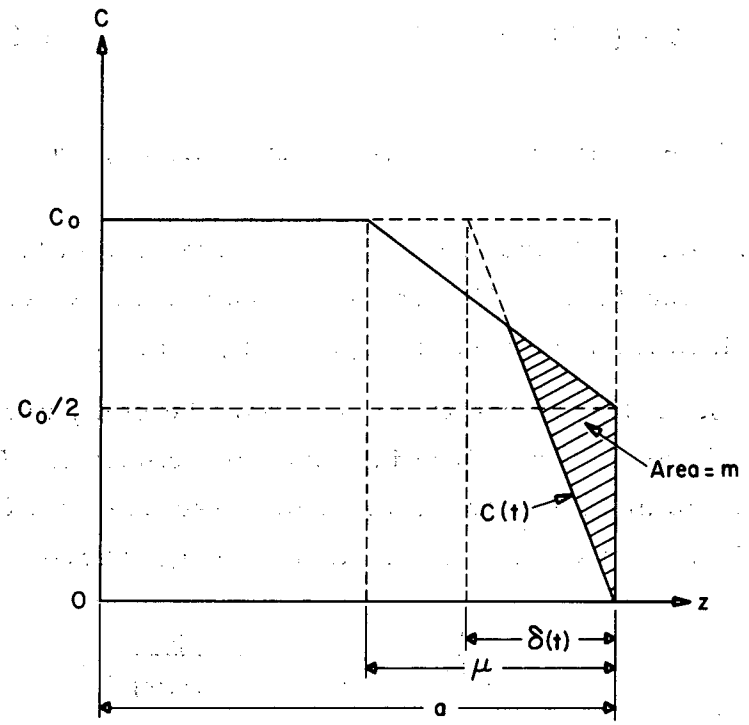

Fig. 28. Straight-line approximation of the concentration profile.

$$\frac{2\,Dt}{\mu^2} = \frac{\delta}{2\mu - \delta} - \ln\left(1 + \frac{\delta}{2\mu - \delta}\right) \quad \text{for } \delta \leq \mu, \qquad \text{(E-3a)}$$

$$\delta = (4\,Dt - \mu + 2\mu \ln 2)^{1/2} \quad \text{for } \delta \geq \mu. \qquad \text{(E-3b)}$$

A correction factor Λ is now defined, where

Λ = (fractional release from a specimen with a uniform initial concentration)/(fractional release from a specimen with initial concentration depleted by recoil). (E-4)

The denominator of this factor may now be computed from Eqs. (E-1) and (E-3), and the problem is solved in principle. The Λ (the f in the notation of Inthoff and Zimen) is presented as a function of κ (of f' in the notation of Inthoff and Zimen), where

$$\kappa = \frac{4}{\pi^{1/2}} \frac{1}{\Lambda\theta}, \quad \theta = \frac{\mu}{2(Dt)^{1/2}}. \qquad \text{(E-5)}$$

Discussion.

Let Λ as calculated from the result of Appendix B be denoted as Λ_1. We have shown that

$$\Lambda_1 = \frac{2}{1 + \Phi}. \qquad \text{(E-6)}$$

Let Λ as calculated by the method of Inthoff and Zimen be denoted as Λ_2. From Eq. (III-3) and Eq. (E-4) we obtain

$$\Lambda_2 = \frac{2C_0}{\pi^{1/2} m} (Dt)^{1/2}; \qquad \text{(E-7)}$$

Λ_2 can be computed now from Eqs. (E-1), (E-3), and (E-7). It can be shown that

$$\lim_{\kappa \to 0} \Lambda_2 = \frac{4}{\pi^{1/2}} , \tag{E-8a}$$

$$\lim_{\kappa \to \infty} \Lambda_2 = \frac{2}{\pi^{1/2}} . \tag{E-8b}$$

Equation (E-8a) is at variance with Eqs. (13) and (20) in the work of Inthoff and Zimen, which give a value of 2 for the same limit. It was proved in our work (and also supported by a physical argument in Appendix B) that the limits of Λ when $\kappa \to 0$ and $\kappa \to \infty$ are 2 and 1 respectively. The function Λ_3, however, defined as

$$\Lambda_3 = \frac{\pi^{1/2}}{2} \Lambda_2, \tag{E-9}$$

goes to the correct value at both limits.

The numerical values of Λ as obtained by Inthoff and Zimen[11] are denoted as Λ_4.

The four functions Λ_1, Λ_2, Λ_3, and Λ_4 are plotted in Fig. 29. Notice that Λ_1 and Λ_3 are almost identical throughout the entire range of κ.

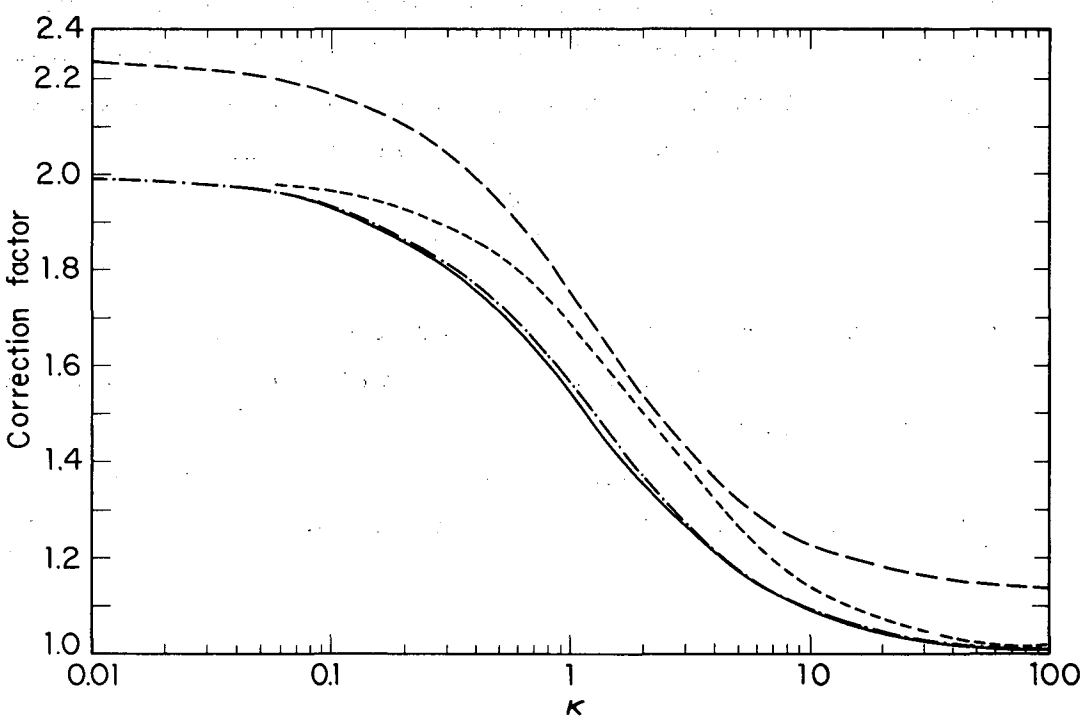

Fig. 29. Λ = Ratio of fractional release from a specimen with a uniform initial concentration to fractional release from a specimen with an initial concentration depleted by recoil.

——— $\Lambda_1 = \Lambda$ as calculated by the method developed in App. B.

— — $\Lambda_2 = \Lambda$ as calculated by using the method of Inthoff and Zimen.

—·—· $\Lambda_3 = \frac{\sqrt{\pi}}{2} \Lambda_2 \quad (\sqrt{\pi}/2)\ \Lambda_2$

----- $\Lambda_4 = \Lambda$ as calculated by Inthoff and Zimen.

Appendix F

COMMENTS ON THE USE OF SURFACE AREA (AS MEASURED BY GAS ADSORPTION) IN THE CALCULATION OF THE DIFFUSION COEFFICIENT IN POSTIRRADIATION ANNEAL OF POWDERS

1. Let the powder consist of N groups. All particles in the nth group are of identical size. Also let

f = fractional release,

f_n = fractional release in the nth group,

a_n = radius of particles in the nth group (cm),

g_n = weight fraction of the nth group,

ρ = density (theoretical) of powder material (g/cm^3),

F = specific surface of powder (cm^2/g),

D = diffusion coefficient (cm^2/sec),

D_F = diffusion coefficient calculated from F (cm^2/sec),

t = time since start of anneal (sec).

2. Assuming the usual "spherical model,"

$$f = \sum_{n=1}^{N} g_n f_n = \frac{6}{\pi^{1/2}} (Dt)^{1/2} \sum_{n=1}^{N} \frac{g_n}{a_n} , \qquad (F\text{-}1)$$

which applies as long as $\frac{Dt}{a^2} < 0.01$.

From the specific surface F,

$$F = \sum_{n=1}^{N} \frac{g_n}{\frac{4}{3}\pi a_n^3 \rho} 4\pi a_n^2 = \frac{3}{\rho} \sum_{n=1}^{N} \frac{g_n}{a_n} , \qquad (F\text{-}2)$$

and from Eqs. (F-1) and (F-2),

$$D_F = \frac{\pi}{4\rho^2} \frac{f^2}{t} \frac{1}{F^2} .$$

Let the groups be arranged in such a way that $a_n < a_{n+1}$ for any n. Let now a_s (where $s < N$) be small enough so that all spheres of groups $1 \cdots s$ will become appreciably depleted during the anneal. The effective surface area for release will decrease then and will be

$$F_{eff} \approx \frac{3}{\rho} \sum_{n=s+1}^{N} \frac{g_n}{a_n} \qquad (F\text{-}4)$$

and

$$D \approx \frac{\pi}{4\rho^2} \frac{f^2}{t} \frac{1}{F_{eff}^2} \; ; \qquad (F\text{-}5)$$

Therefore

$$\frac{D}{D_F} \approx \left[\frac{\sum_{n=1}^{N} \frac{g_n}{a_n}}{\sum_{n=s+1}^{N} \frac{g_n}{a_n}} \right]^2 \qquad (F\text{-}6)$$

3. Numerical example

Let $g_1 = 0.3$,

$g_2 = 0.7$,

$\frac{a_2}{a_1} = 50$,

$$\therefore \quad \frac{D}{D_F} = \left[\frac{0.3 + \frac{0.7}{50}}{\frac{0.7}{50}} \right]^2 = 500.$$

In order for this to happen a release of the order of g_1, or approximately 30%, should be observed.

4. Auskern and Osawa's experiment[A2]

D reported by Auskern and Osawa is only 1/500 to 1/1000 the D found here (Fig. 23).

The powder used by Auskern and Osawa had

$$F = 2600 \text{ cm}^2/\text{g},$$

hence

$$a = \left[\sum_{n=1}^{N} \frac{g_n}{a_n} \right]^{-1} = \frac{3}{\rho F} \approx \frac{3}{14 \times 2600} \approx 0.8 \text{ micron.}$$

Auskern and Osawa reported that in some runs the slope of the plot of f vs $t^{1/2}$ was continuously decreasing during the first 20 hours. Anneals lasted 50 to 100 hours and slope was measured at the latter part of the anneal. Fractional release was as high as 30%. Hence the above numerical example demonstrates how the depletion discussed above could have accounted for the low reported values of D.

NOMENCLATURE

a Characteristic dimension; half thickness in case of a slab, radius in case of a cylinder (cm)

C Concentration of tracer atoms (atoms/cm^3)

C_0 Concentration of tracer atoms in the internal region (which is not depleted by recoil) before diffusion started (atoms/cm^3)

D Diffusion coefficient for the tracer atoms (cm^2/sec)

D_0 Frequency factor (cm^2/sec)

f Fractional release via process of diffusion (dimensionless) Eq. (III-2)

g Auxiliary function defined in Eqs. (B-8) and (B-37), for slab and cylindrical geometries

E Activation energy (calories/mole)

G Green's function for diffusion with zero concentration on the boundaries

Its Laplace transform is given by Eqs. (B-7) and (B-36) for slab and cylindrical geometries

h Half height of a finite cylinder (cm)

M Recoil correction function for the diffusion coefficient (dimensionless) (see Fig. 11)

p Argument of the Laplace transform Eq. (B-5)

P Probability, Eq. (A-21)

q Square root of p, Eq. (B-5)

Q Number of tracer atoms. Slab: in units of $2aC_0$ cm^2 in a parallelepiped that cuts a unit area at each face of the slab; cylinder: in units of $\pi a^2 C_0$ cm in a unit height of the cylinder.

Q_0 Initial value of Q -- i.e., before diffusion started.

r Space coordinate in cylindrical geometry (cm)

R Gas constant, 1987 Cal/mole/°K.

S Dimensionless initial concentration, Eq. (B-10)

t Time since start of diffusion (sec)

U Dimensionless concentration, Eq. (B-2)

v Dimensionless variable

V A function for which a Laplace transform exists but otherwise arbitrary

w Integration variable

x Dimensionless length, Eq. (B-2)

z Space coordinate in slab geometry (cm)

Z Solution of the diffusion equation in a slab with thickness 2a and with recoil-depleted initial concentration

α Dimensionless quantity defined by Eq. (B-53)

β Dimensionless quantity defined by Eq. (B-53)

γ Dimensionless quantity defined by Eq. (B-53)

Λ Correction factor, defined by Eq. (E-4)

δ Error in initial concentration of a cylindrical surface due to the neglecting of curvature, defined by Eq. (A-14)

ϵ Dimensionless recoil range, Eq. (A-11)

κ Dimensionless quantity, $\kappa = 4/\pi^{1/2}\Lambda\theta)$

θ Dimensionless quantity, $\theta = \epsilon/(2\tau^{1/2})$

μ Fission recoil range of a tracer atom or its parent (cm) (see discussion in Appendix A. 1)

ρ Solution of the diffusion equation in an infinite cylinder with radius a and with a recoil-depleted initial concentration

τ Dimensionless time, Eq. (B-2)

Φ Dimensionless quantity, Eq. (B-75)

BIBLIOGRAPHY

A1. C. B. Alcock and P. Grieveson, A Study of Uranium Borides and Carbides by Means of the Knudsen Effusion Technique, IAEA, Vienna May, 1962.

A2. A. Auskern and Y. Osawa, Xenon Diffusion in Uranium Carbide Powder, BNL-6012, 1962.

B1. J. Belle, Uranium Dioxide: Properties and Nuclear Applications (U. S. Atomic Energy Commission, Washington D. C., July 1961).

B2. G. Berthier, "Problèms theoretiques liés a la determination des coefficients d' autodiffusion dans les solides par la methode des exchanges isotopiques heterogènes", J. Chim. Phys. 49, 527 (1952).

B3. H. A. Bethe and J. Ashkin, The Passage of Heavy Particles through Matter, in Experimental Nuclear Physics, edited by E. Segrè (John Wiley & Sons Inc., New York) Vol. 1, page 230.

B4. J. O. Blomeke, Nuclear Properties of U^{235} Fission Products, ORNL-1783, November 1955.

B5. A. H. Booth and G. T. Rymer, Determination of Diffusion Constant of Fission Xenon in UO_2 Crystals and Sintered Compacts, AECL-692, Aug. 1958.

C1. H. S. Carslaw and J. C. Jaeger, Conduction of Heat in Solids (Oxford University Press, London, 1959).

C2. B. L. Cohen, A. F. Cohen, and C. D. Coley, Energy Distribution of Mass-97 Fission Fragments From Thermal Neutron Fission of U^{235}, Phys. Rev. 104, 4, 1046 (1956).

C3. J. Crank, The Mathematics of Diffusion (Oxford University Press, London, 1956).

D1. R. F. Dickerson (Battelle Memorial Institute), private communication.

E1. J. D. Eichenberg, P. W. Frank, T. J. Kisiel, B. Lustman, and K. H. Vogel, Effects of Irradiation of Bulk Uranium Dioxide, WAPD-183, Oct. 1957.

F1. P. Fong, Statistical Theory of Nuclear Fission: Asymmetric Fission, Phys. Rev. 102, 2, 434 (1956).

G1. 40 MW(E) Prototype High Temperature Gas Cooled Reactor, Research and Development Program, GA-2747, March 1962.

G2. William Goldsworthy, Recording Pulse-Height Analyzer, UCRL-2083, Jan. 1953.

G3. D. E. Gray, editor, American Institute of Physics Handbook (McGraw-Hill Book Co., Inc. New York, 1957).

H1. R. C. Hawkings and W. J. Edwards, Apparatus for Routine Quantitative Estimation of Radionuclides by γ-Scintillation Spectrometry, AECL-819 Nov. 1958.

H2. F. B. Hildebrand, Advanced Calculus for Engineers (Prentice Hall, Inc., Englewood Cliffs, New Jersey, 1958), p. 185.

H3. H. B. Huntington and F. Seitz, Mechanism for Self-Diffusion in Metallic Copper, Phys. Rev. 61, 315 (1942).

I1. K. Inthoff and K. E. Zimen, Kinetik der Diffusion radioaktiver Edelgase aus festen Stoffen nach Bestrahlung, Transactions of Chalmers University of Technology, Gothenburg, Sweden, No. 176 (1956).

J1. S. C. Jain, Simple Solutions of the Partial Differential Equation for Diffusion, in Proc. Roy. Math. Soc. (London), p. 359 (1957).

J2. W. Jost, Diffusion in Solids, Liquids and Gases (Academic Press, Inc., New York, 1952).

K1. J. Kaye, A Table of the First Eleven Repeated Integrals of the Error Function, J. Math. Phys. 34, 119 (1955).

K2. W. D. Kingery, Introduction to Ceramics (John Wiley & Sons, Inc., New York, 1960).

L1. D. Lazarus, Diffusion in Metals, Solid State Physics 10, 71 (1960).

L2. W. B. Lewis, The Retrun of Fission Product Gases to UO_2, AECL-964, Jan. 1960.

L3. A. B. Lidiard and K. Tharmalingam, Diffusion Processes at Low Temperatures, Discussions Faraday Soc. No. 28 (1959).

L4. R. Lindner and H. Matzke, Diffusion radioaktiver Edelgase in Uranoxyden und Uranmonokarbid, Z. Naturforsch. 14a, 1074-1077 (1959).

P1 D. E. Poland, J. W. Green, and J. L. Margrave, Corrected Optical Pyrometer Readings, NBS Monograph 30, April 1961.

R1. D. V. Ragone, private communication (General Atomic).

R2. F. A. Rough and W. Chubb, An Evaluation of Data on Nuclear Carbides, BMI-1441, May 1960.

S1. R. Smoluchowski, Movement and Diffusion Phenomena in Grain Boundaries, in Imperfection in Nearly Perfect Crystals, W. Shockley, Chairman of Editorial Committee (John Wiley & Sons, Inc., New York, 1950).

S2. W. H. Stephens, J. R. MacEwan, and A. M. Ross, The Diffusion Behavior of Fission Xenon in Uranium Dioxide, TID-7610, Oct. 1960.

V1. W. Volk, Applied Statistics for Engineers (McGraw-Hill Book Co., Inc., New York, 1958).

W1. M. A. Weinberg and P. E. Wigner, The Physical Theory of Neutron Chain Reactors, (University of Chicago Press, Chicago, 1958).

This report was prepared as an account of Government sponsored work. Neither the United States, nor the Commission, nor any person acting on behalf of the Commission:

A. Makes any warranty or representation, expressed or implied, with respect to the accuracy, completeness, or usefulness of the information contained in this report, or that the use of any information, apparatus, method, or process disclosed in this report may not infringe privately owned rights; or

B. Assumes any liabilities with respect to the use of, or for damages resulting from the use of any information, apparatus, method, or process disclosed in this report.

As used in the above, "person acting on behalf of the Commission" includes any employee or contractor of the Commission, or employee of such contractor, to the extent that such employee or contractor of the Commission, or employee of such contractor prepares, disseminates, or provides access to, any information pursuant to his employment or contract with the Commission, or his employment with such contractor.